Ice-free geomorphometry of Queen Maud Land, East Antarctica: 2. Prince Olav Coast

I.V. Florinsky

iflor@mail.ru

Institute of Mathematical Problems of Biology, Keldysh Institute of Applied Mathematics, Russian Academy of Sciences https://orcid.org/0000-0003-1273-5912

S.O. Zharnova

National Research Tomsk State University https://orcid.org/0009-0002-1420-3741

Research Article

Keywords: topography, digital elevation model, mathematical modeling, Antarctica

Posted Date: August 22nd, 2025

DOI: https://doi.org/10.21203/rs.3.rs-7428671/v1

Additional Declarations: The authors declare no competing interests.

Ice-free geomorphometry of Queen Maud Land, East Antarctica: 2. Prince Olav Coast

I.V. Florinsky[1*], S.O. Zharnova[2]

[1] Institute of Mathematical Problems of Biology, Keldysh Institute of Applied Mathematics, Russian Academy of Sciences, Pushchino, Moscow Region, 142290, Russia

[2] National Research Tomsk State University, 36 Lenin Ave., Tomsk, 634050, Russia

Abstract

Geomorphometric modeling and mapping of ice-free Antarctic areas can be applied for obtaining new quantitative knowledge about the topography of these unique landscapes and for the further use of morphometric information in Antarctic research. Within the framework of a project of creating a physical geographical thematic scientific reference geomorphometric atlas of ice-free areas of Antarctica, we performed geomorphometric modeling and mapping of key ice-free areas of the Prince Olav Coast (Queen Maud Land, East Antarctica). These include the Cape Hinode, Polkanov Hills (Cape Ryûgû), and Tereshkova Oasis (Sinnan Rocks). As input data, we used three fragments of the Reference Elevation Model of Antarctica (REMA). For the three ice-free areas and adjacent glaciers, we derived models and maps of eleven, most scientifically important morphometric variables (i.e., slope, aspect, horizontal curvature, vertical curvature, minimal curvature, maximal curvature, catchment area, topographic wetness index, stream power index, total insolation, and wind exposition index). The obtained models and maps describe the ice-free topography of the Prince Olav Coast in a rigorous, quantitative, and reproducible manner. New morphometric data can be useful for further geological, geomorphological, glaciological, ecological, and hydrological studies of this region.

Keywords: topography, digital elevation model, mathematical modeling, Antarctica

1 Introduction

There are three main types of ice-free areas in Antarctica: (1) Antarctic oases, i.e. coastal, shelf, and mountainous ice-free areas; (2) ice-free islands (or areas thereof) situated outside the ice shelves; and (3) ice-free mountain chains (or their portions) and nunataks (Markov et al., 1970; Simonov, 1971; Korotkevich, 1972; Alexandrov, 1985; Pickard, 1986; Beyer and Bölter, 2002; Sokratova, 2010).

Geomorphometry deals with the mathematical modeling and analysis of topography as well as relationships between topography and other components of geosystems (Evans, 1972; Moore et al., 1991; Wilson and Gallant, 2000; Shary et al., 2002; Hengl and Reuter, 2009; Minár et al., 2016; Florinsky, 2017, 2025a). Geomorphometric modeling and mapping of ice-free Antarctic areas (Florinsky, 2023a, 2023b; Florinsky and Zharnova, 2025a, 2025b) can be used for obtaining new quantitative knowledge about the topography of these terrains and for the further use of morphometric information in solving problems of geomorphology, geology, glaciology, soil science, ecology, and other sciences. A project has recently been launched to create a physical geographical thematic scientific reference geomorphometric atlas of ice-free areas of Antarctica (Florinsky, 2024, 2025b).

Currently, as part of this project, we carry out a geomorphometric modeling and mapping of ice-free areas of Queen Maud Land, East Antarctica. Previously, we published series of geomorphometric maps for the Sôya Coast of that land (Florinsky and Zharnova, 2025b). In this paper, we present results for key ice-free areas of the Prince Olav Coast.

* Correspondence to: iflor@mail.ru

2 Study areas

The Prince Olav Coast is the easternmost coast of Queen Maud Land, East Antarctica. It is located between Lützow-Holm Bay to the west and Alasheev Bight to the east, between 67.9°S and 68.9°S, and 40°E and 44.7°E (Fig. 1). It is bordered on the west by the Sôya Coast and on the east by Enderby Land. The Prince Olav Coast is about 250 km long. It consists of a margin of the ice sheet, several outlet glaciers, and a chain of small ice-free coastal areas.

The Prince Olav Coast was discovered in 1930 by the Norwegian expedition of H. Riiser-Larsen and named after the Norwegian prince, later King Olav V of Norway. In 1957–1977, ice-free areas of the Prince Olav Coast were intensively studied by members of the Soviet Antarctic Expedition and the Japanese Antarctic Research Expedition (Tatsumi and Kikuchi, 1959; Markov et al., 1962; Znachko-Yavorsky and Klimov, 1963; Znachko-Yavorsky, 1964; Kamenev et al., 1965; Klimov, 1965; Alexandrov, 1973, 1985; Yanai and Ishikawa, 1978; Nakai et al., 1979; Hiroi et al., 1983; Yoshida, 1983; Sokratova, 2010).[1]

In this paper, we consider three key ice-free areas of the Prince Olav Coast (Fig. 1, Table 1), from west to east: the Cape Hinode (Fig. 2a), Polkanov Hills (Cape Ryûgû) (Fig. 2b), and Tereshkova Oasis (Sinnan Rocks) (Fig. 2c).

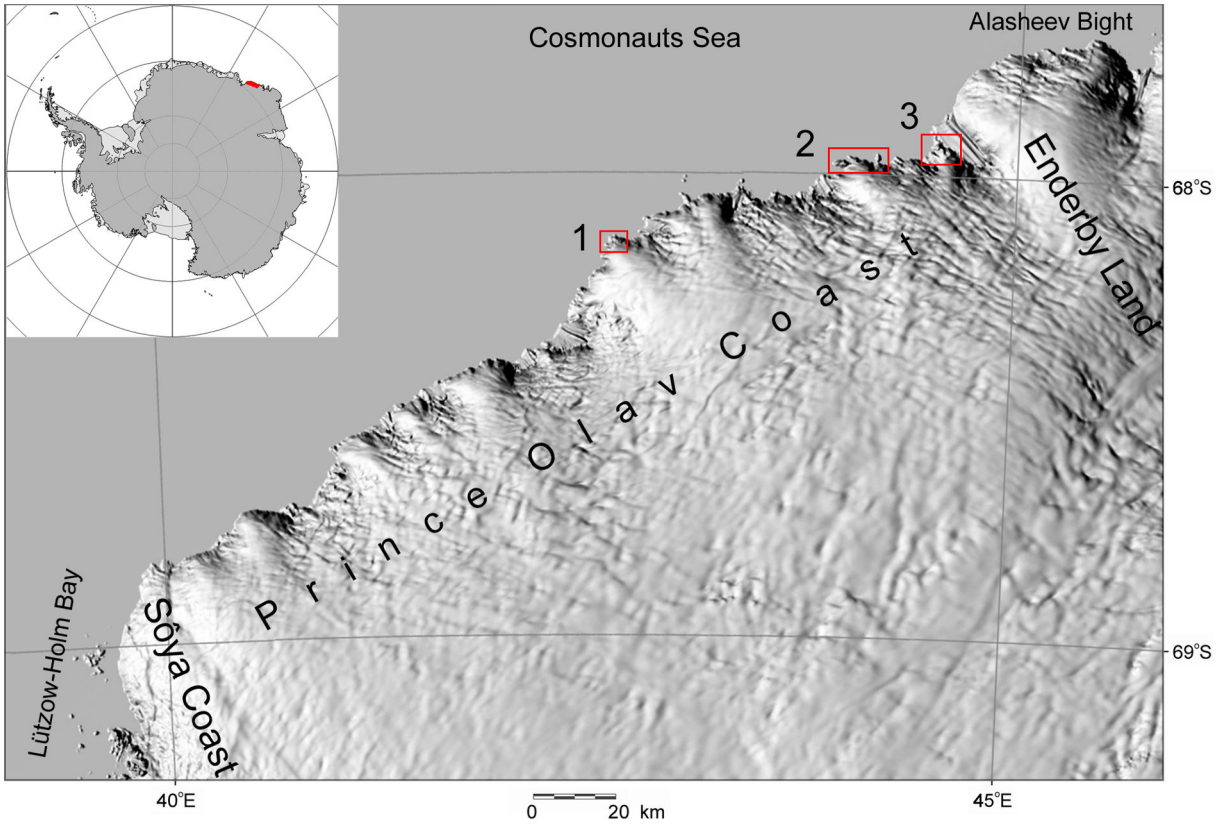

Fig. 1 Geographical location of the study areas: 1 – Cape Hinode, 2 – Polkanov Hills (Cape Ryûgû), 3 – Tereshkova Oasis (Sinnan Rocks). The hill-shaded map was produced by REMA Explorer (PGC, 2022–2024).

[1] Due to this past activity, some geographical features of the eastern part of the Prince Olav Coast (including two study areas) have double names assigned by both the Soviet and Japanese cartographic authorities (Bakaev and Tolstikov, 1966; Tolstikov, 1969; Yanai and Ishikawa 1978; Nakai et al., 1980; Hiroi et al., 1983; Alexandrov, 1985; Donidze, 1987; GSI, 1990; Korotkevich et al., 2005). In such cases, we use names of the both origin, Russian and Japanese (in brackets).

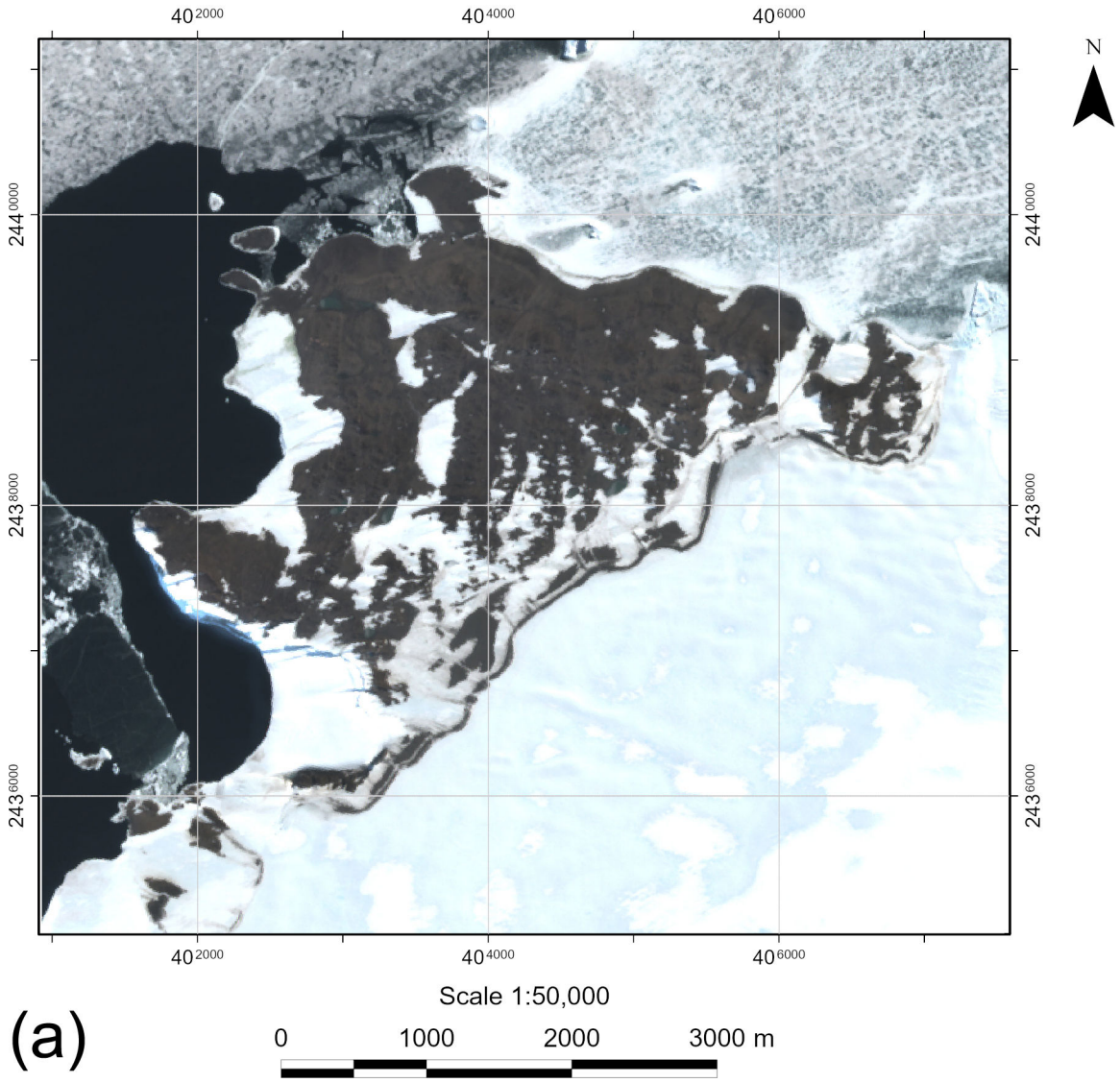

Fig. 2 Satellite images of the study areas: (a) Cape Hinode.

(Continued)

Table 1 Characteristics of the study areas (Fig. 1) and their DEMs.

#	Area name	Geographical coordinates	Area, km^2	DEM size, m	DEM size, point	Points with elevation values
1	Cape Hinode	68.15075° S, 42.68939° E	12.2	9,032 × 8,080	1,129 × 1,010	505,756
2	Polkanov Hills (Cape Ryûgû)	67.97402° S, 44.06999° E	13.8	12,728 × 5,496	1,591 × 687	515,277
3	Tereshkova Oasis (Sinnan Rocks)	67.95424° S, 44.55420° E	23.1	9,520 × 7,544	1,190 × 943	957,573

The Cape Hinode is a small rock area with typical elevations of 70–130 m above sea level (ASL). The Polkanov Hills (Cape Ryûgû) are two strips of rocky coastal hills with elevations of 100–130 m ASL. The Tereshkova Oasis (Sinnan Rocks) is a rocky hill terrain with typical heights of 50–150 m ASL. These areas are separated from each other by the ice sheet and outlet glaciers, and are bounded to the south and/or southeast by the ice sheet and to the north and/or northwest by the Cosmonauts Sea of the Southern Ocean.

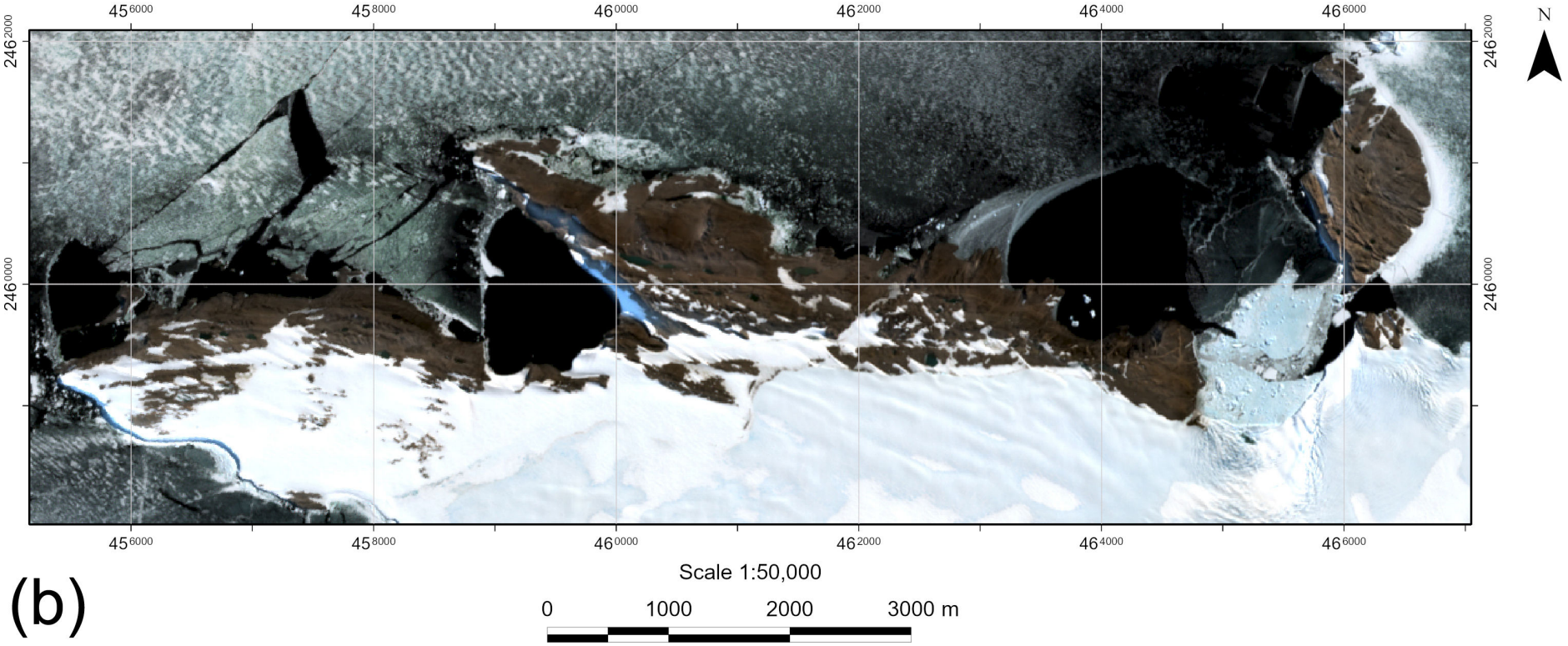

Fig. 2, cont'd Satellite images of the study areas: (b) Polkanov Hills (Cape Ryûgû).

(Continued)

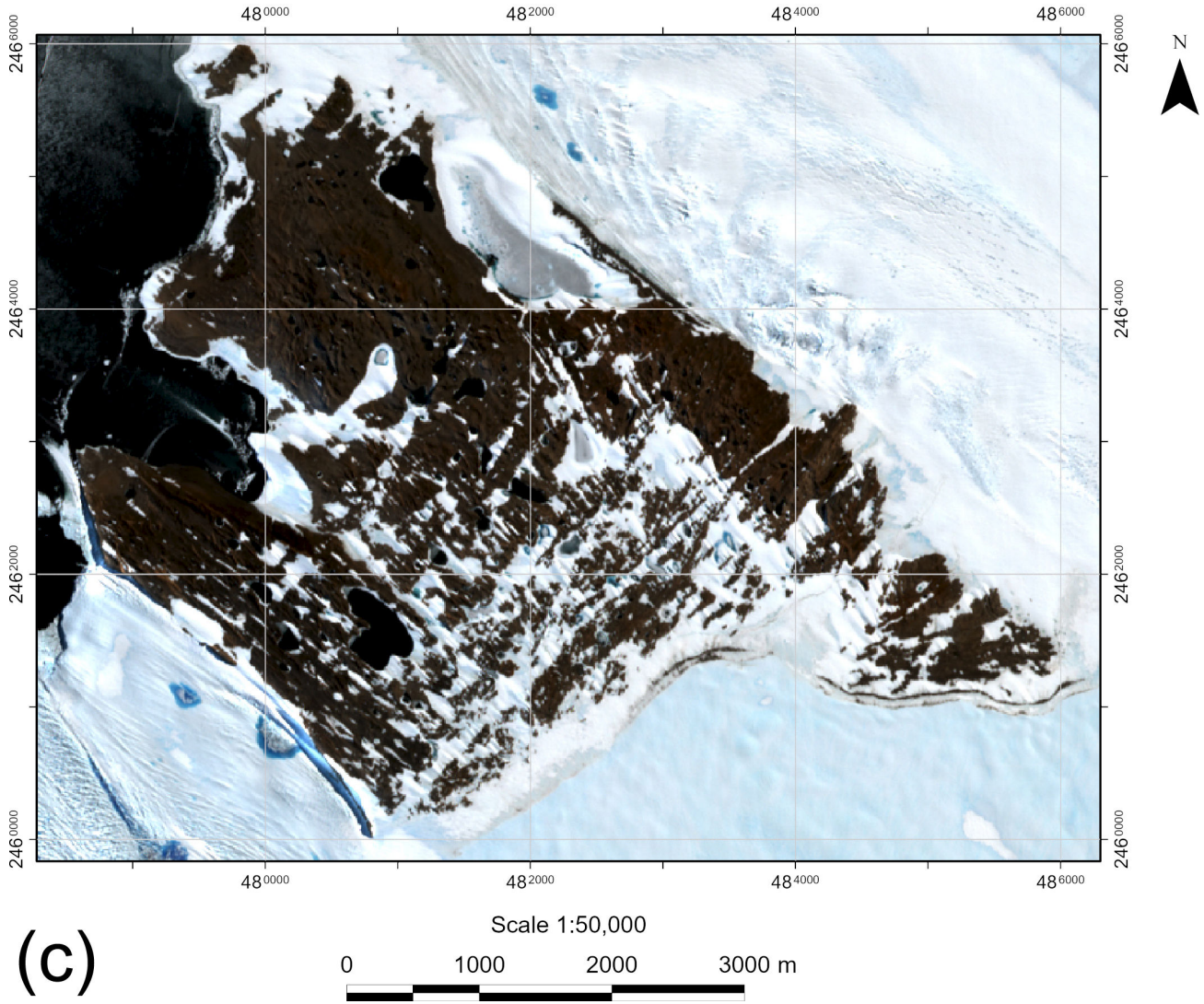

Fig. 2, cont'd Satellite images of the study areas: (c) Tereshkova Oasis (Sinnan Rocks).
Fragments of a Sentinel-2A MSI scene, 05.02.2025 (ESA, 2025). True color synthesis with brightness and contrast enhancement. UTM projection (zone 38S).

Geomorphically, the study areas are characterized by glaciated landforms including *roches moutonnee*, U-shaped valleys, and troughs. In particular, the Cape Hinode has a low undulating surface including small hills and depressions. In the Polkanov Hills (Cape Ryûgû), there are the U-shaped, east-west stretching valleys with glacial morainic deposits and many ponds. In the Tereshkova Oasis (Sinnan Rocks), a shallow and broad glacial trough, continuing Ermak Bay (Kagami Inlet), divides the oasis into the southwestern and the northeastern parts. The undulating surface of the oasis, including small crests and depressions filled with lakes, descends gradually from its inner margin to the sea. Within the study areas, the landforms are greatly controlled by the geological structures of bedrocks (Znachko-Yavorsky and Klimov, 1963; Alexandrov, 1973; Yoshida, 1983).

The ice-free areas of the Prince Olav Coasts are generally composed of Precambrian to Cambrian gneisses and granites. In particular, the Cape Hinode area is characterized by anorthositic gneiss. Subordinate rocks include garnet gneiss, hornblende gneiss, amphibolites, granites, and calc-silicate rocks. The basement rocks exposed in the Polkanov Hills (Cape Ryûgû) are biotite, garnet-biotite, biotite-hornblende, and siliceous gneisses with subordinate metabasites, granites, pegmatites, and aplites. The Tereshkova Oasis (Sinnan Rocks) is underlain by gneisses and granitic migmatites along with granites and pegmatites. In the ice-free areas of the Prince Olav Coasts, glacial drifts, fluvioglacial deposits, and unconsolidated marine sediments are widely distributed (Tatsumi and Kikuchi, 1959; Znachko-Yavorsky, 1964; Kamenev et al., 1965; Klimov, 1965; Yanai and Ishikawa, 1978; Nakai et al., 1979, 1980; Hiroi et al., 1983).

3 Materials and methods

We used three digital elevation models (DEMs) with a grid spacing of 8 m. The DEMs were extracted from the Reference Elevation Model of Antarctica (REMA) (Howat et al., 2019; REMA, 2018–2022). For data processing and mapping, we applied a procedure described earlier in our papers (Florinsky, 2025b; Florinsky and Zharnova, 2025b).

3.1 Preprocessing

REMA is presented in the polar stereographic projection with an elevation datum of the WGS84 ellipsoid. There is no bathymetry in REMA; such cells have ‘no data’ values. The extracted DEMs were reprojected into the UTM projection (zone 38S) preserving the original 8-m grid spacing (Table 1). Ellipsoidal elevations were transformed into orthometric ones.

3.2 Calculations

Digital models of eleven, most scientifically important morphometric variables were derived from the reprojected DEMs. The list of morphometric variables (Table 2) includes six local attributes: slope (G), aspect (A), horizontal curvature (k_h), vertical curvature (k_v), minimal curvature (k_{min}), and maximal curvature (k_{max}); one nonlocal variable—catchment area (CA); two combined variables: topographic wetness index (TWI) and stream power index (SPI); as well as two two-field-specific attributes—total insolation ($TIns$) and wind exposition index (WEx). Formulas and detailed interpretations of these morphometric variables can be found elsewhere (Shary et al., 2002; Florinsky 2017, 2025a, chap. 2).

To derive digital models of local variables, we used a finite-difference method by Evans (1980). To compute models of CA, we applied a maximum-gradient based multiple flow direction algorithm by Qin et al. (2007) to preprocessed sink-filled DEMs. CA digital models were then logarithmized. To derive digital models of combined morphometric variables, we used calculated models of CA and G. To compute digital models of two-field-specific attributes, we applied two related methods by Böhner (2004). $TIns$ were estimated for one mid-summer day (1st January) with a temporal step of 0.5 h.

Table 2 Definitions and interpretations of key morphometric variables (Shary et al., 2002; Florinsky, 2017, 2025a, chap. 2).

Variable, notation, and unit	Definition and interpretation
	Local morphometric variables
Slope, G (°)	An angle between the tangential and horizontal planes at a given point of the topographic surface. Relates to the velocity of gravity-driven flows.
Aspect, A (°)	An angle between the north direction and the horizontal projection of the two-dimensional vector of gradient counted clockwise, from 0° to 360°, at a given point of the topographic surface. Relates to the direction of gravity-driven flows
Horizontal (tangential) curvature, k_h (m^{-1})	A curvature of a normal section tangential to a contour line at a given point of the surface. A measure of flow convergence and divergence. Gravity-driven lateral flows converge where $k_h < 0$, and diverge where $k_h > 0$. k_h mapping reveals crest and valley spurs.
Vertical (profile) curvature, k_v (m^{-1})	A curvature of a normal section having a common tangent line with a slope line at a given point of the surface. A measure of relative deceleration and acceleration of gravity-driven flows. They are decelerated where $k_v < 0$, and are accelerated where $k_v > 0$. k_v mapping reveals terraces and scarps.
Minimal curvature, k_{min} (m^{-1})	A curvature of a principal section with the lowest value of curvature at a given point of the surface. $k_{min} > 0$ corresponds to local convex landforms, while $k_{min} < 0$ relates to elongated concave landforms (e.g., hills and troughs, correspondingly).
Maximal curvature, k_{max} (m^{-1})	A curvature of a principal section with the highest value of curvature at a given point of the surface. $k_{max} > 0$ corresponds to elongated convex landforms, while $k_{max} < 0$ relate to local concave landforms (e.g., crests and holes, correspondingly).
	Nonlocal morphometric variables
Catchment area, CA (m^2)	An area of a closed figure formed by a contour segment at a given point of the surface and two flow lines coming from upslope to the contour segment ends. A measure of the contributing area.
	Combined morphometric variables
Topographic wetness index, *TWI*	A ratio of catchment area to slope gradient at a given point of the topographic surface. A measure of the extent of flow accumulation.
Stream power index, *SPI*	A product of catchment area and slope gradient at a given point of the topographic surface. A measure of potential flow erosion and related landscape processes.
	Two-field specific morphometric variables
Total insolation, *TIns* (kWh/m^2)	A measure of the topographic surface illumination by solar light flux. Total potential incoming solar radiation, a sum of direct and diffuse insolations.
Wind exposition index, *WEx*	A measure of an average exposition of slopes to wind flows of all possible directions at a given point of the topographic surface.

3.3 Mapping

First, we created hypsometric maps of the key ice-free areas of the Prince Olav Coast from the reprojected DEMs. Two gradient hypsometric tint scales were used:

(1) To display the elevations of the ice-free topography, we applied the green-yellow part of the standard spectral hypsometric scale of color plasticity (Kovaleva, 2014).

(2) To display the elevations of the glacier topography, we utilized a modified hypsometric tint scale for polar regions (Patterson and Jenny, 2011).

Then, two hypsometric tintings was combined with achromatic hill shading derived from the DEMs by a standard procedure (Figs. 3a, 4a, and 5a).

Finally, we put geographical names on the hypsometric maps. As a source of this information, we used available topographic, geological, and landscape maps of the study

areas (Yanai and Ishikawa 1978; Nakai et al., 1980; Hiroi et al., 1983; Alexandrov, 1985; GSI, 1990; Korotkevich et al., 2005).

Second, from the calculated digital morphometric models, we produced three series of morphometric maps for the key ice-free areas of the Prince Olav Coast (Figs. 3b–l, 4b–l, and 5b–l). For optimal visual perception of morphometry, we used the following rules for applying gradient tint scales:

1. *G* and *CA* can take only positive values. To map *G* and *CA*, we applied a standard gray tint scale; the minimum and maximum values of *G* or *CA* correspond to white and black, respectively (Figs. 3b and 3h, 4b and 4h, 5b and 5h).

2. k_h, k_v, k_{min}, and k_{max} can take both negative and positive values, having opposite physical mathematical and physical geographical sense and interpretation. To map curvatures, we used a two-color tint scale consisting of two contrasting parts, blue and orange (negative and positive values, respectively). The most and least saturated shades of blue or orange colors correspond to the absolute maximum and absolute minimum values, respectively, of k_h, k_v, k_{min}, and k_{max} (Figs. 3d–g, 4d–g, 5d–g).

3. *TWI* and *SPI* can take only positive values. To map these indices, we applied a standard spectral tint scale; the minimum and maximum values of *TWI* or *SPI* correspond to violet and red, respectively (Figs. 3i and 3j, 4i and 4j, 5i and 5j).

4. *TIns* is a nonnegative variable. To map it, we used an orange tint scale: the minimum and maximum *TIns* values correspond to the darkest and lightest orange shades depicting the least and most illuminated areas, respectively (Figs. 3k, 4k, and 5k).

5. *WEx* is a positive dimensionless variable, wherein values below and above 1 relate to wind-shadowed and -exposed areas, respectively. To map this index, we applied a two-color tint scale consisting of two contrasting parts, orange and violet (values below and above 1, respectively). The darkest shades of orange and violet colors correspond to the minimum and maximum *WEx* values, respectively, while the lightest shades of the colors correspond to 1 (Figs. 3l, 4l, and 5l).

All maps were produced in 1:50,000 scale.

There is no lake bathymetry data in REMA; lake cells contain interpolated values of lake coastal elevations, that is, artifacts. Also, REMA has multiple island-like artifacts related to icebergs. On the produced maps, the lakes and island-like artifacts were masked.

To create masks, we used maps of three spectral indices, namely, modified normalized difference water index (MNDWI) (Xu, 2006), ferrous minerals ratio (FMR), and iron oxide ratio (IOR) (Segal, 1982). We derived the spectral index maps from a satellite scene captured on 05.02.2025 by the Sentinel-2A multispectral imager (MSI) (ESA, 2025). To map spectral indices, we used composite legends allowing for the most successful classification of objects by moisture level and iron content. For example, MNDWI maps (Fig. A1) display ice and snow in blue, open water bodies and light snow in green, while ice-free rocks in gray. FMR maps (Fig. A2) highlight rocks in red, orange, and yellow. IOR maps (Fig. A3) show open water bodies in gray, ice and snow in green, as well as rock areas in red, orange, and yellow.

For DEM processing and geomorphometric calculations, we used a software SAGA 9.8.1 (Conrad et al., 2015). For morphometric mapping, Sentinel-2A MSI data processing, spectral index mapping, and map masking, we utilized ArcGIS Pro 3.0.1 (ESRI, 2015–2024).

4 Results

Geomorphometric modeling and mapping resulted in the three series of large-scale morphometric maps for the key ice-free areas of the Prince Olav Coast including the Cape Hinode (Fig. 3), Polkanov Hills (Cape Ryûgû) (Fig. 4), and Tereshkova Oasis (Sinnan Rocks) (Fig. 5).

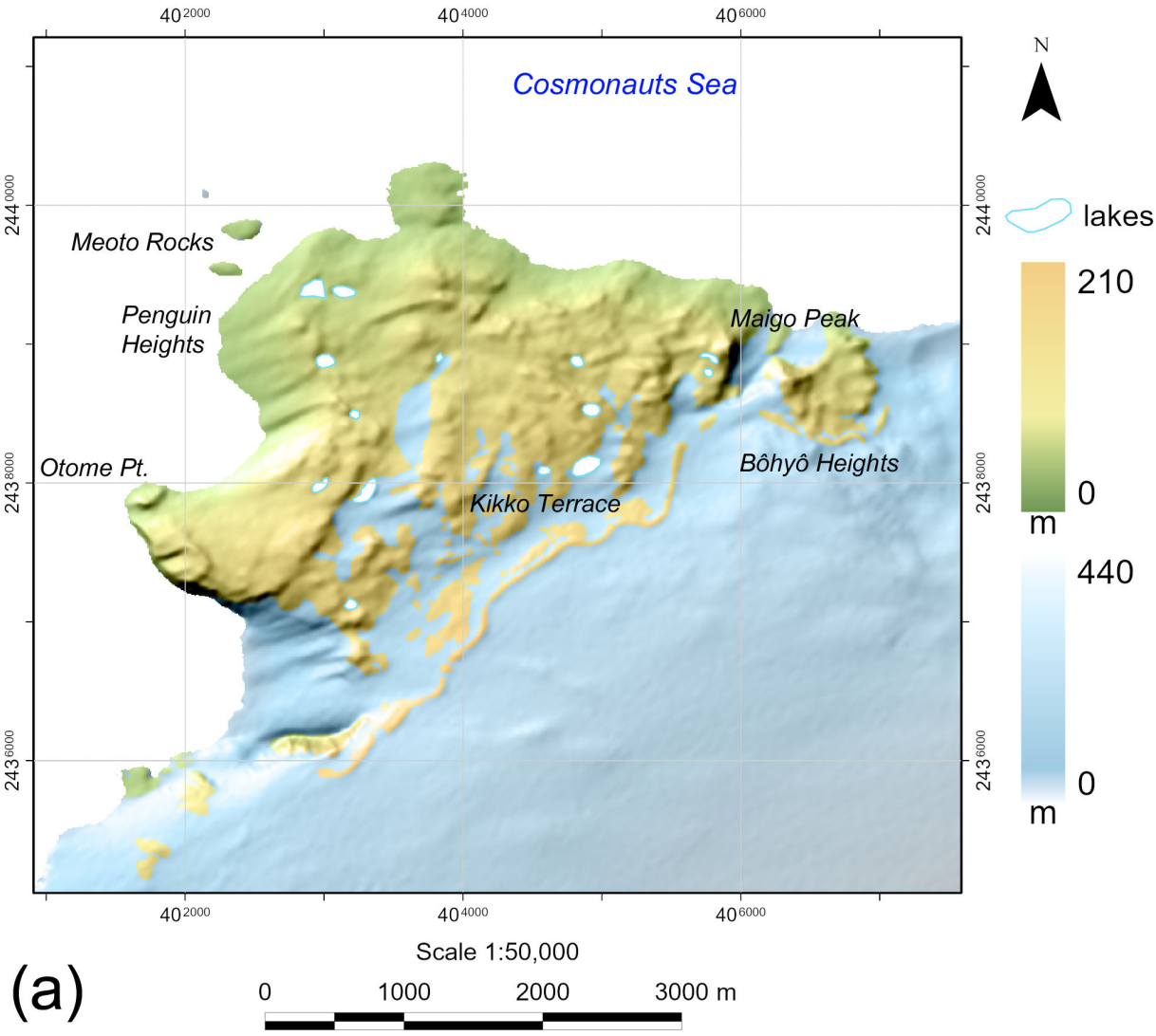

Fig. 3 Cape Hinode: (a) Elevation.

(Continued)

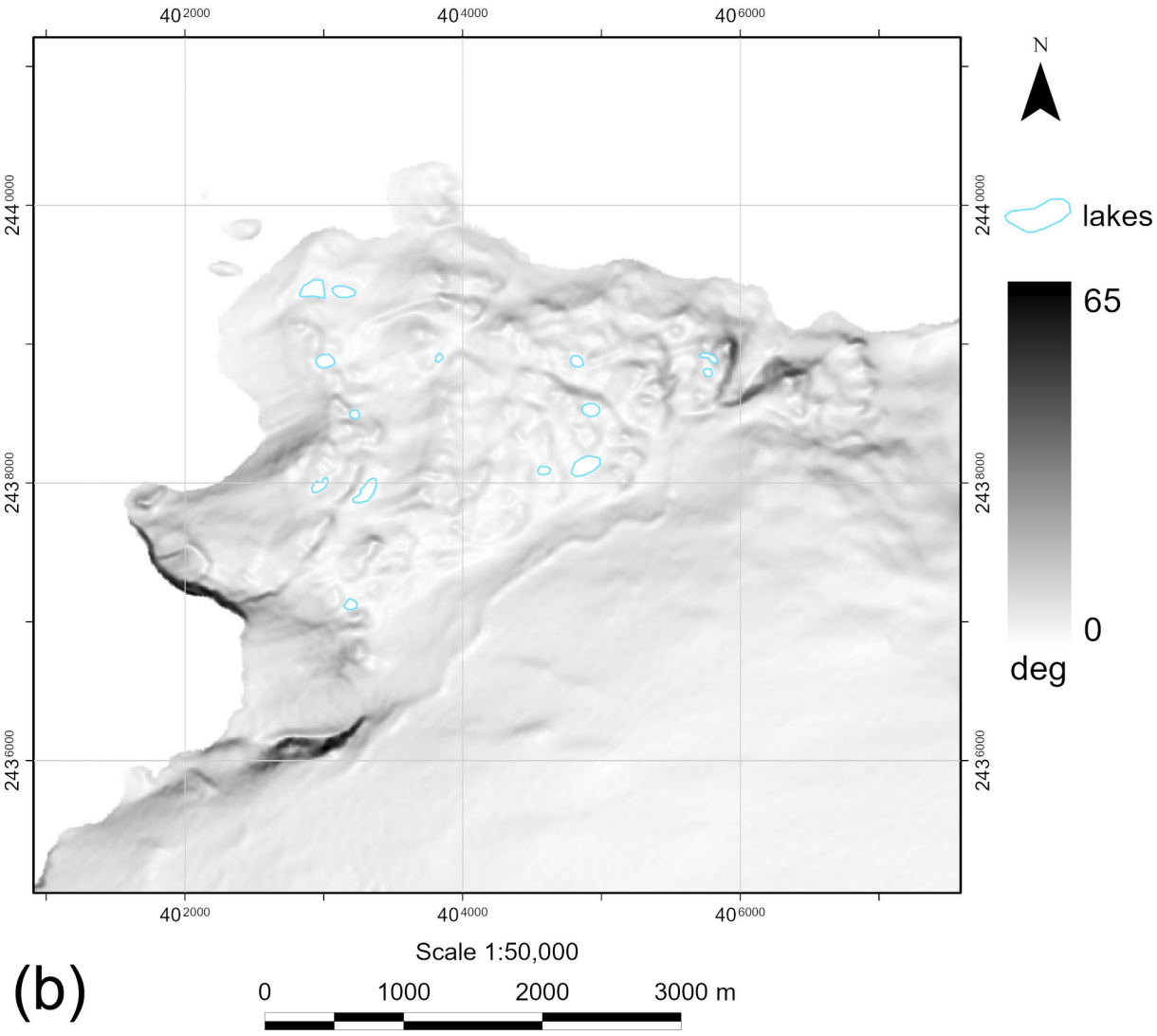

Fig. 3, cont'd Cape Hinode: (b) Slope.

(Continued)

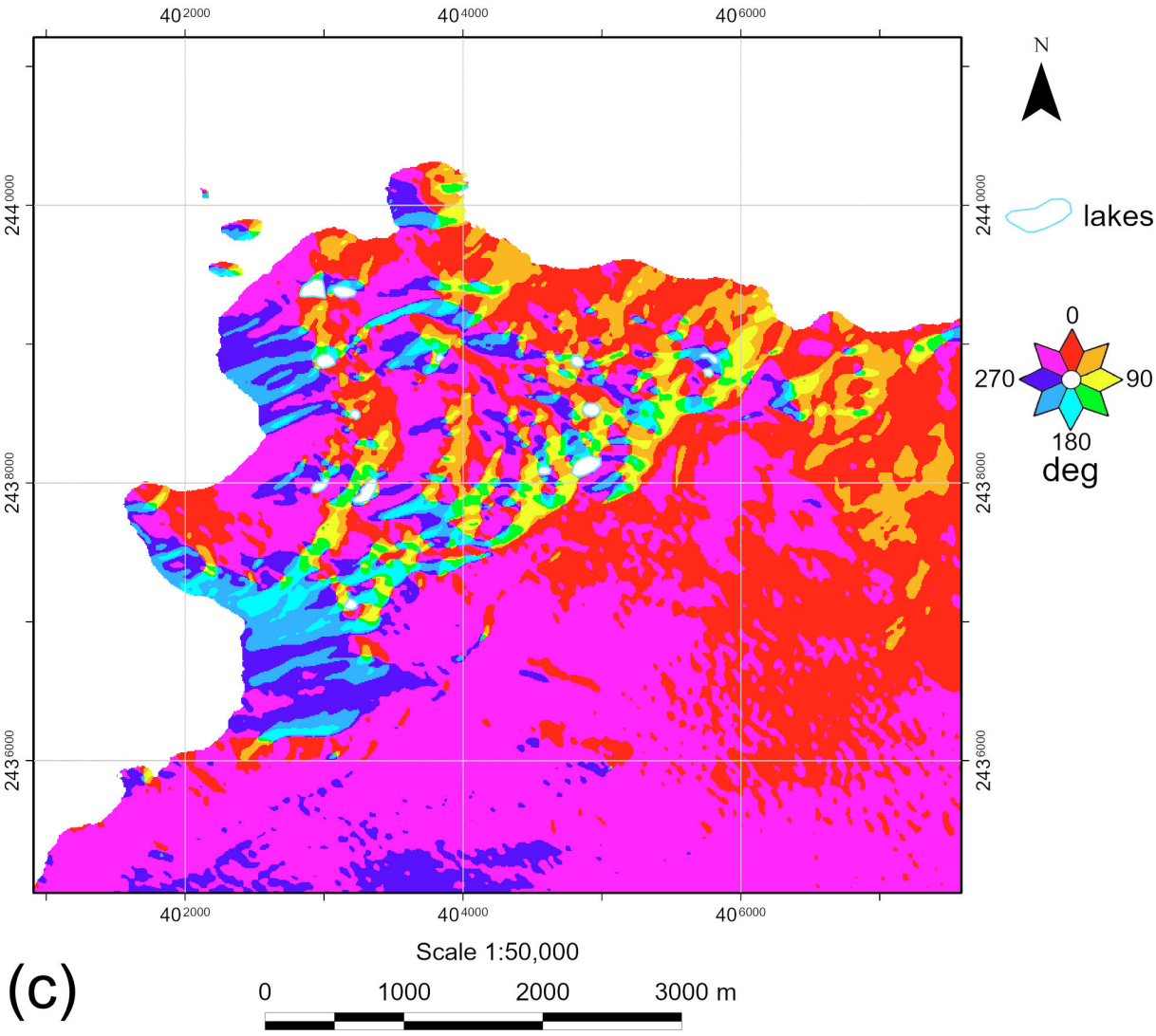

Fig. 3, cont'd Cape Hinode: (c) Aspect.

(Continued)

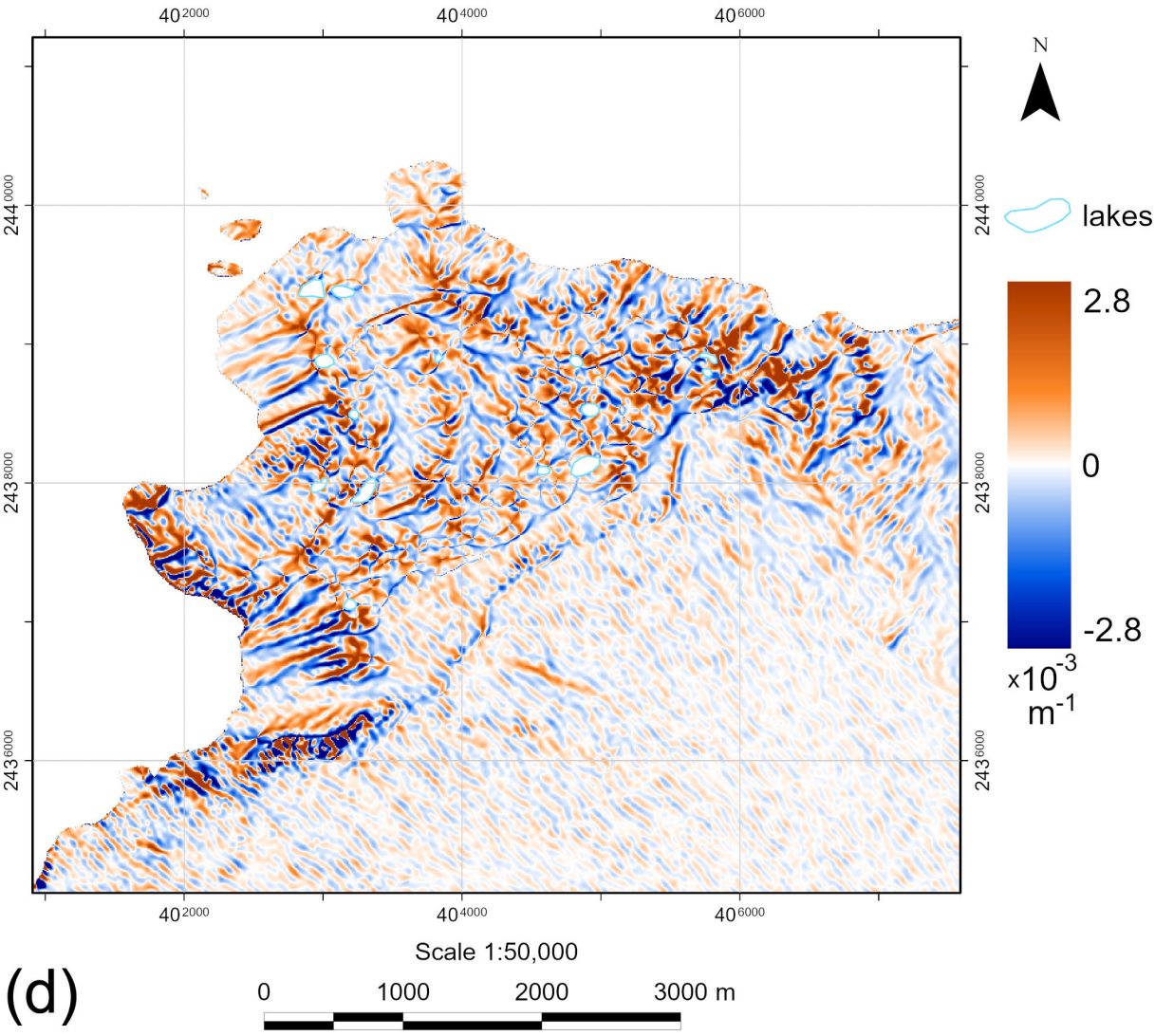

Fig. 3, cont'd Cape Hinode: (d) Horizontal curvature.

(Continued)

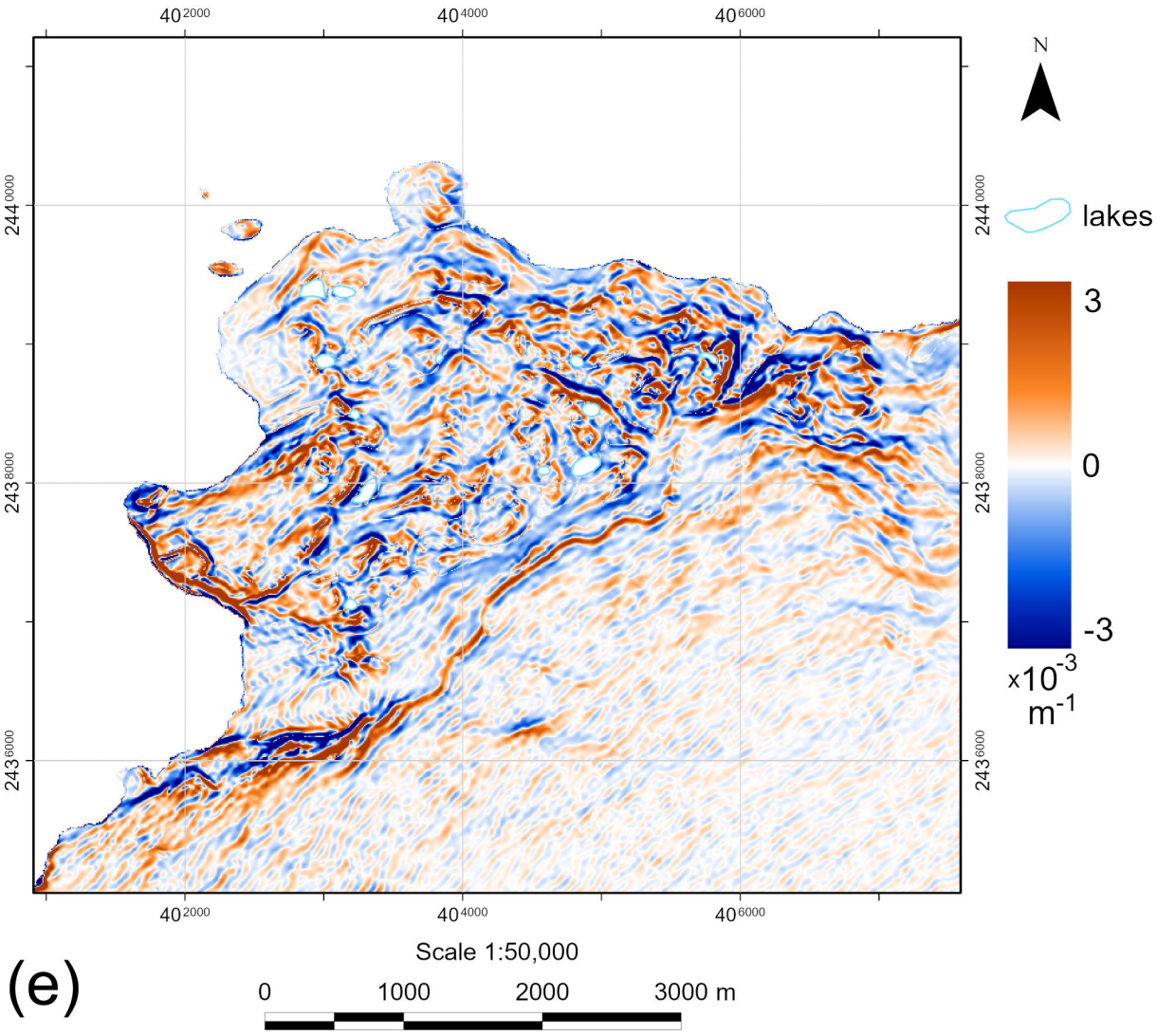

Fig. 3, cont'd Cape Hinode: (e) Vertical curvature.

(Continued)

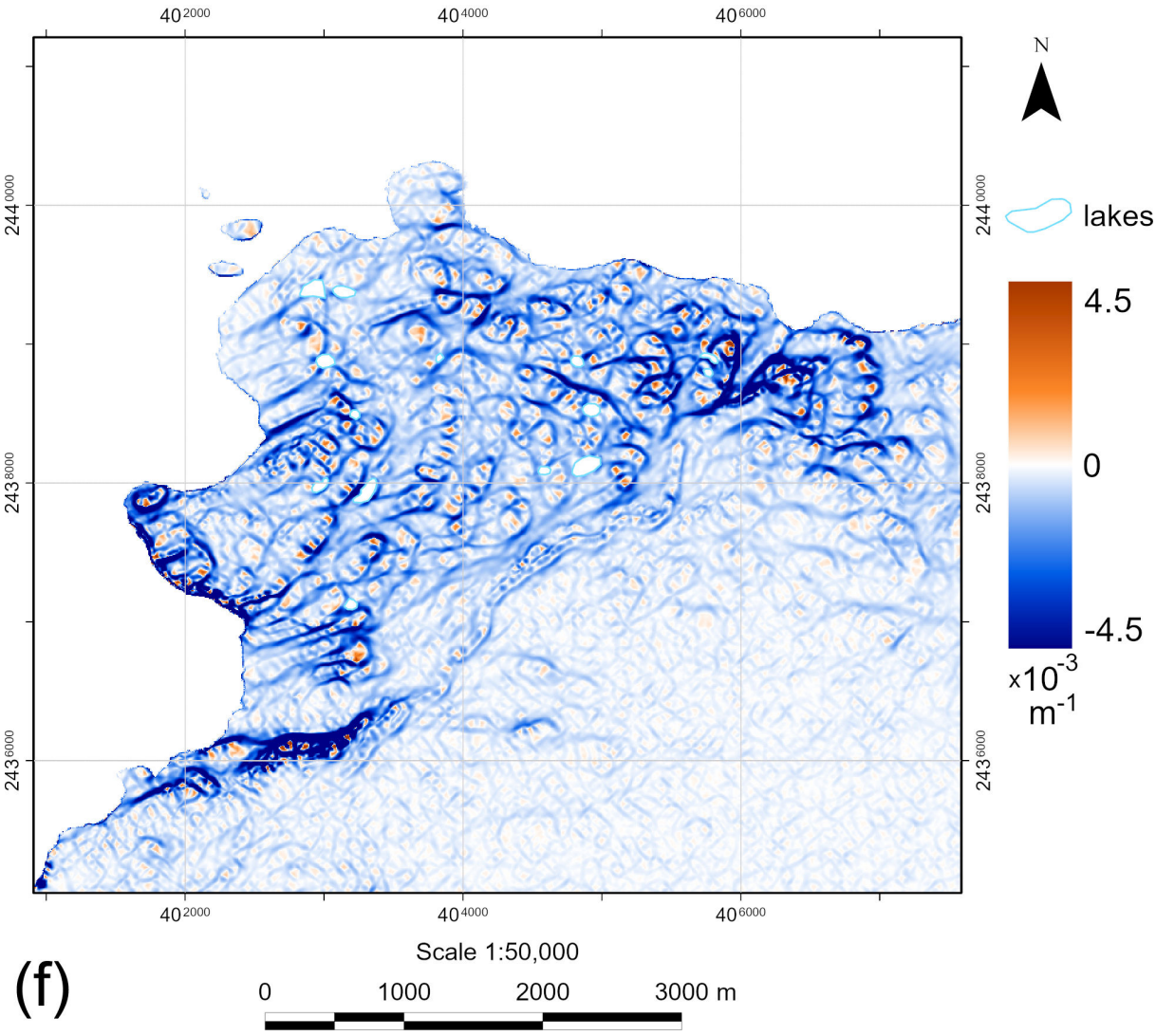

Fig. 3, cont'd Cape Hinode: (f) Minimal curvature.

(Continued)

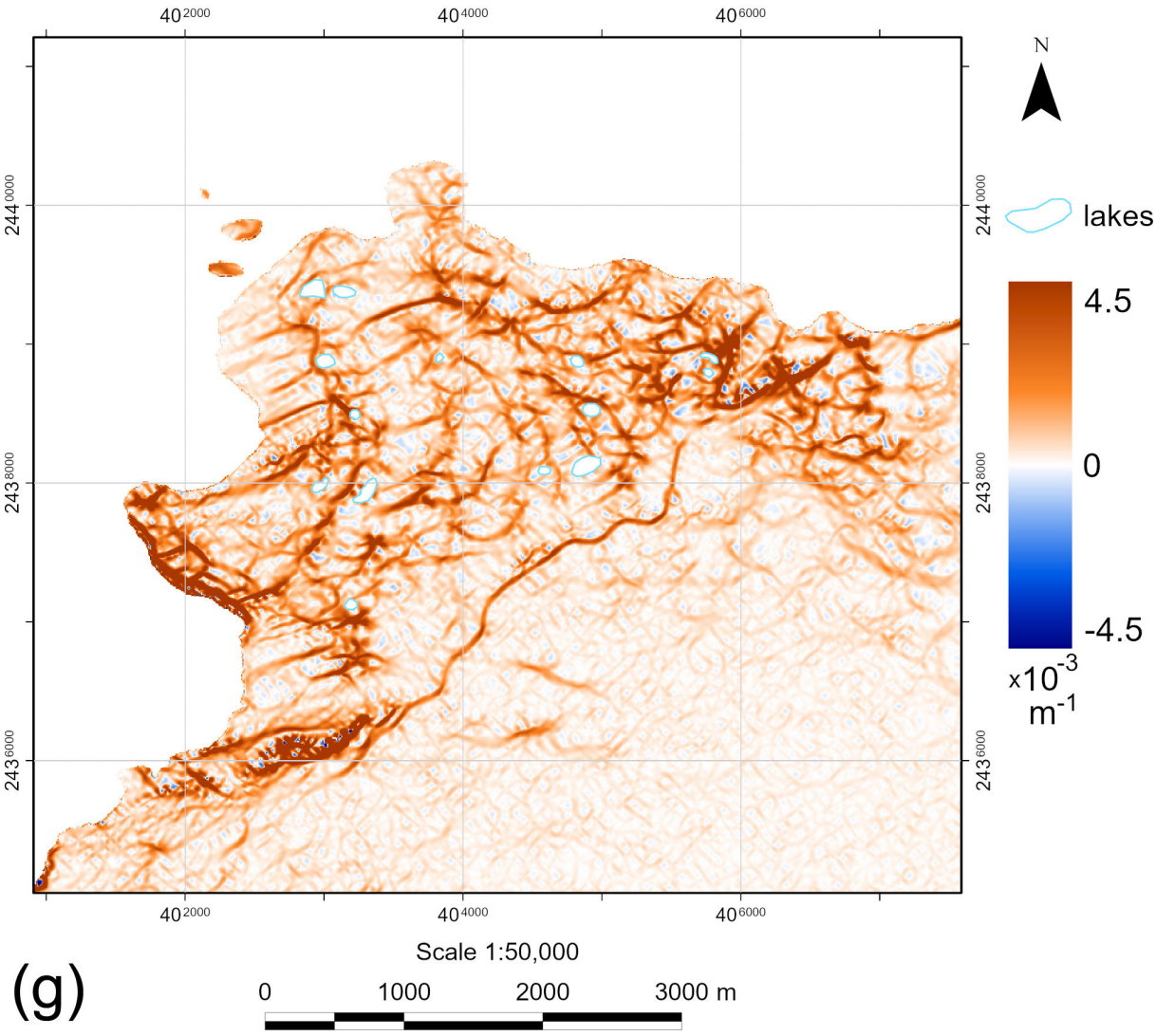

Fig. 3, cont'd Cape Hinode: (g) Maximal curvature.

(Continued)

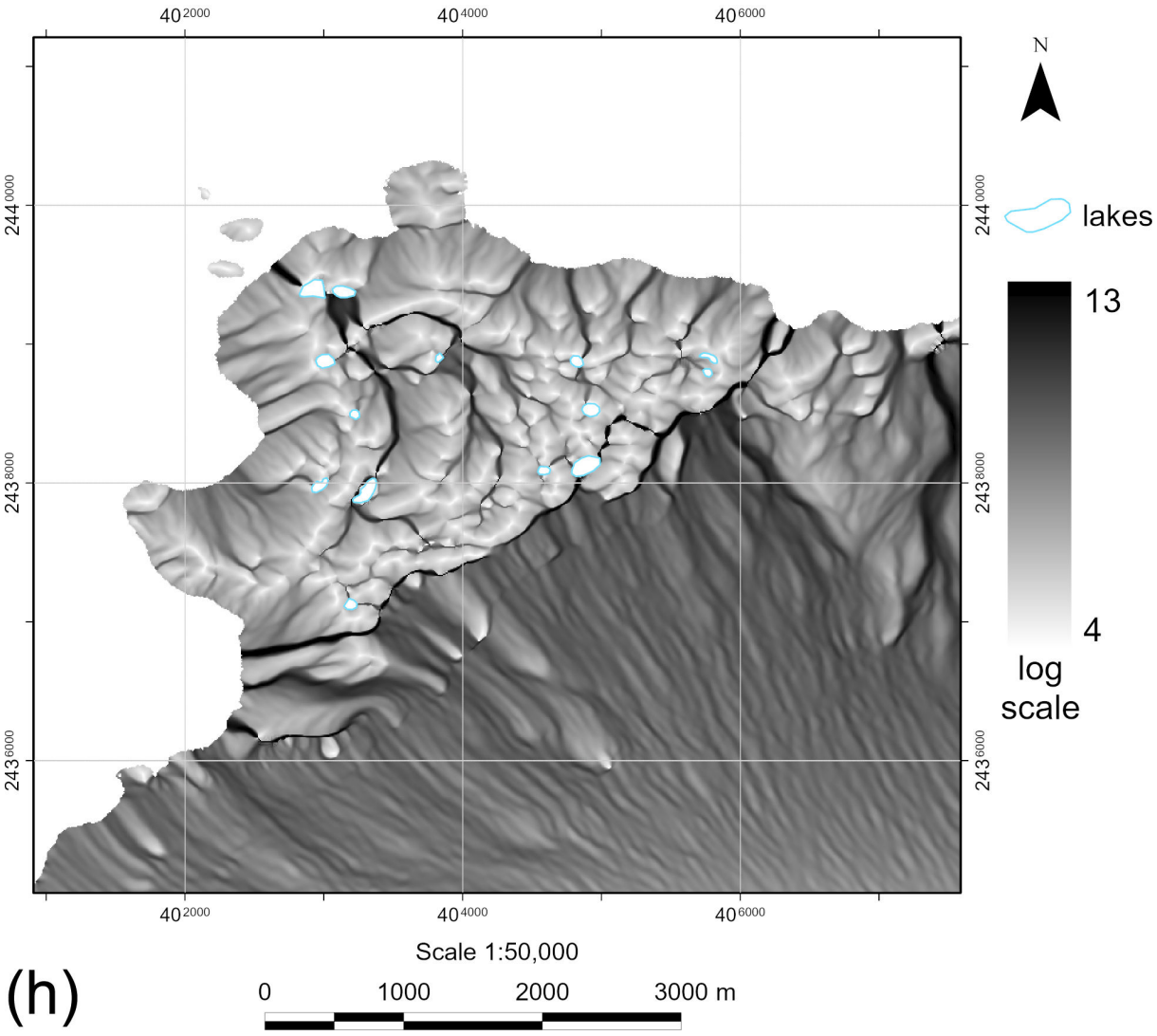

Fig. 3, cont'd Cape Hinode: (h) Catchment area.

(Continued)

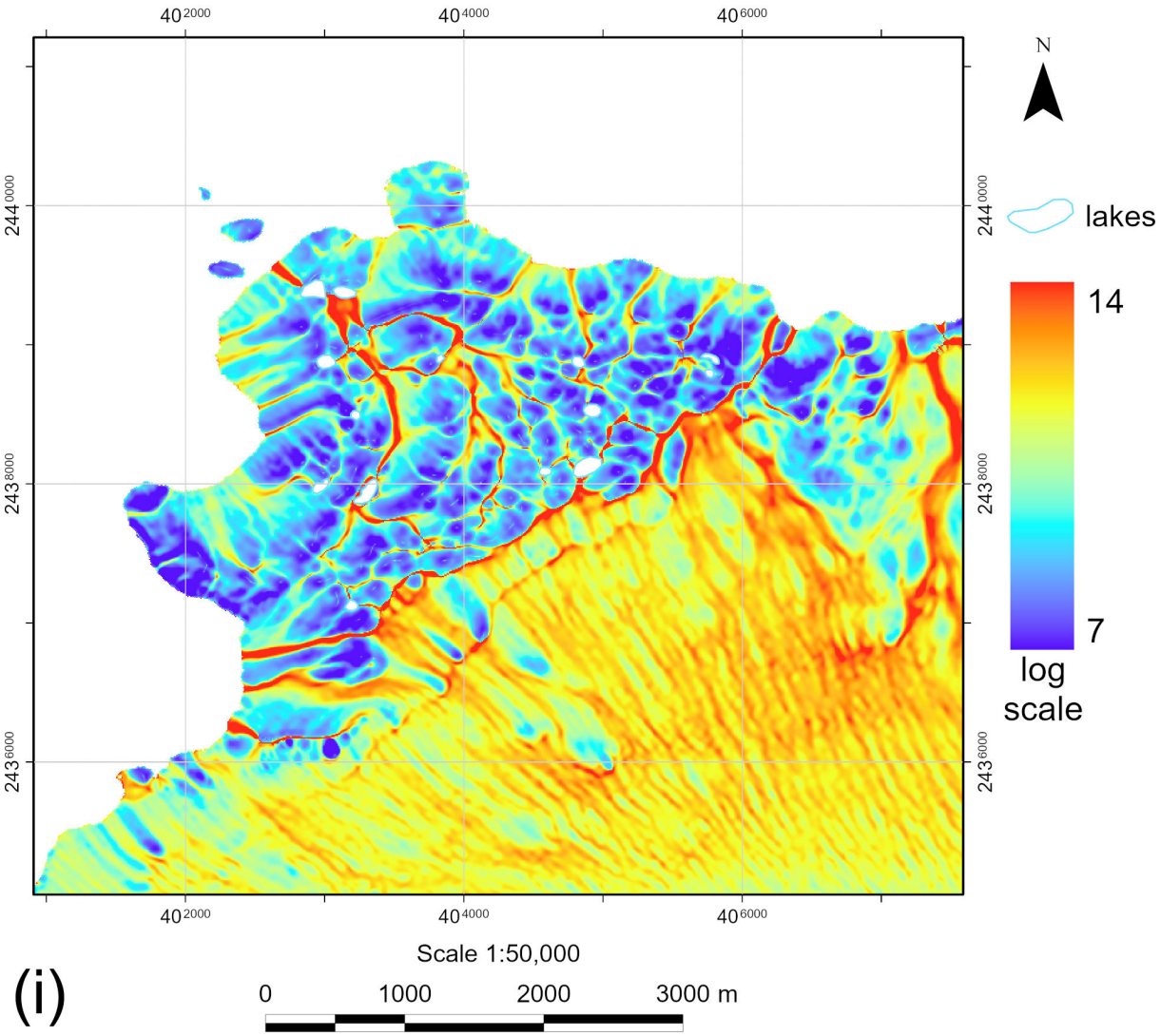

Fig. 3, cont'd Cape Hinode: (i) Topographic wetness index.

(Continued)

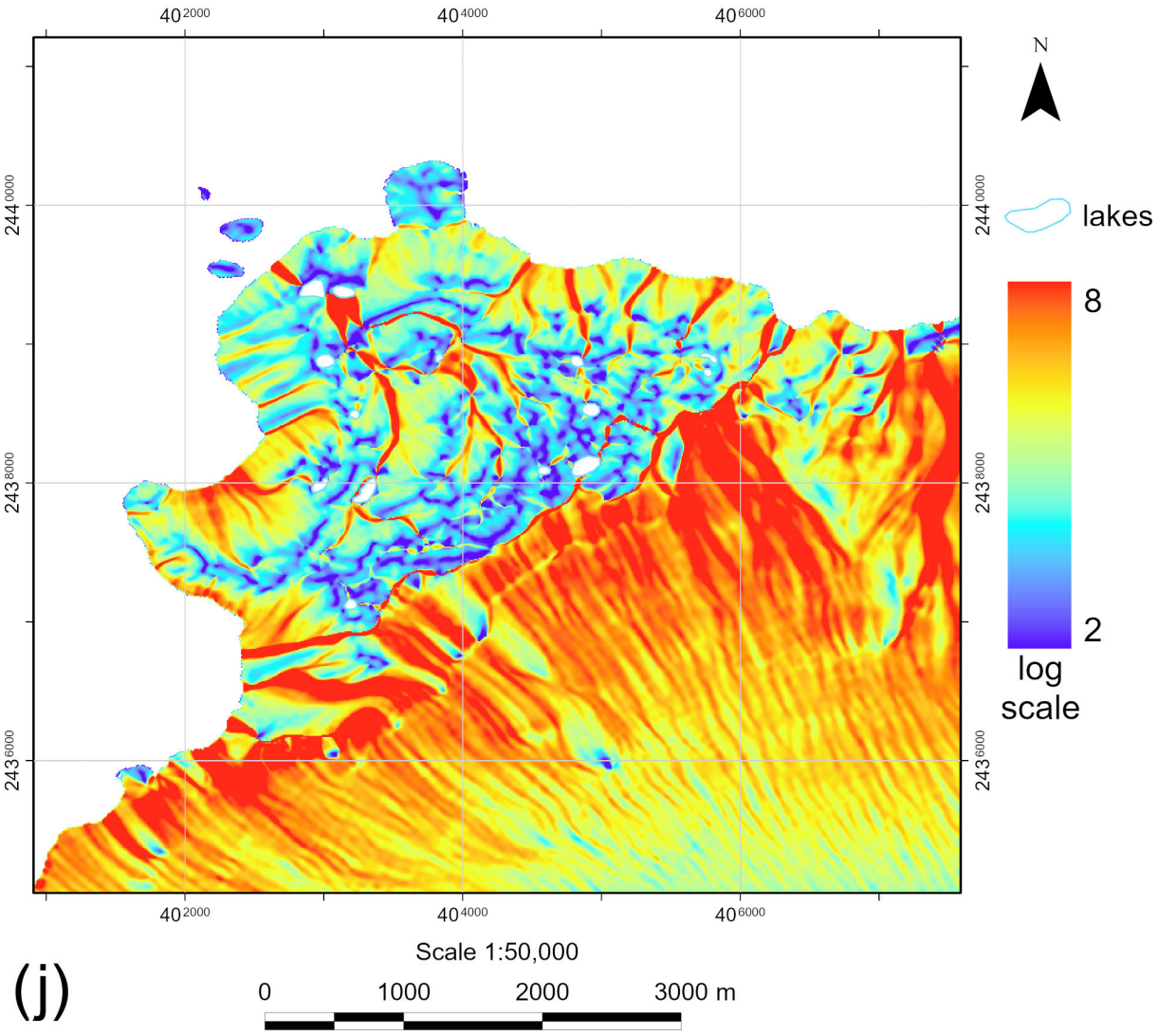

Fig. 3, cont'd Cape Hinode: (j) Stream power index.

(Continued)

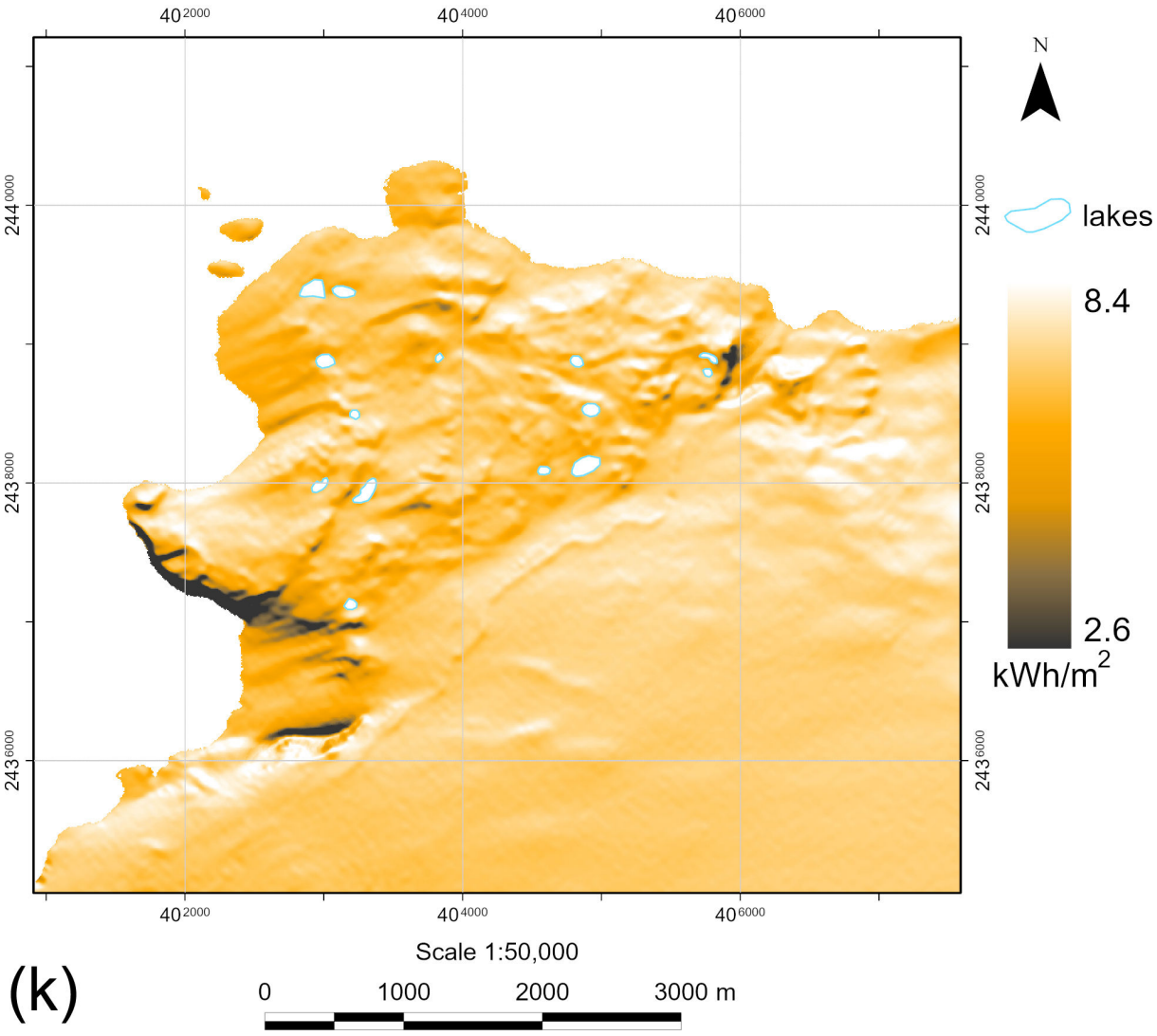

Fig. 3, cont'd Cape Hinode: (k) Total insolation.

(Continued)

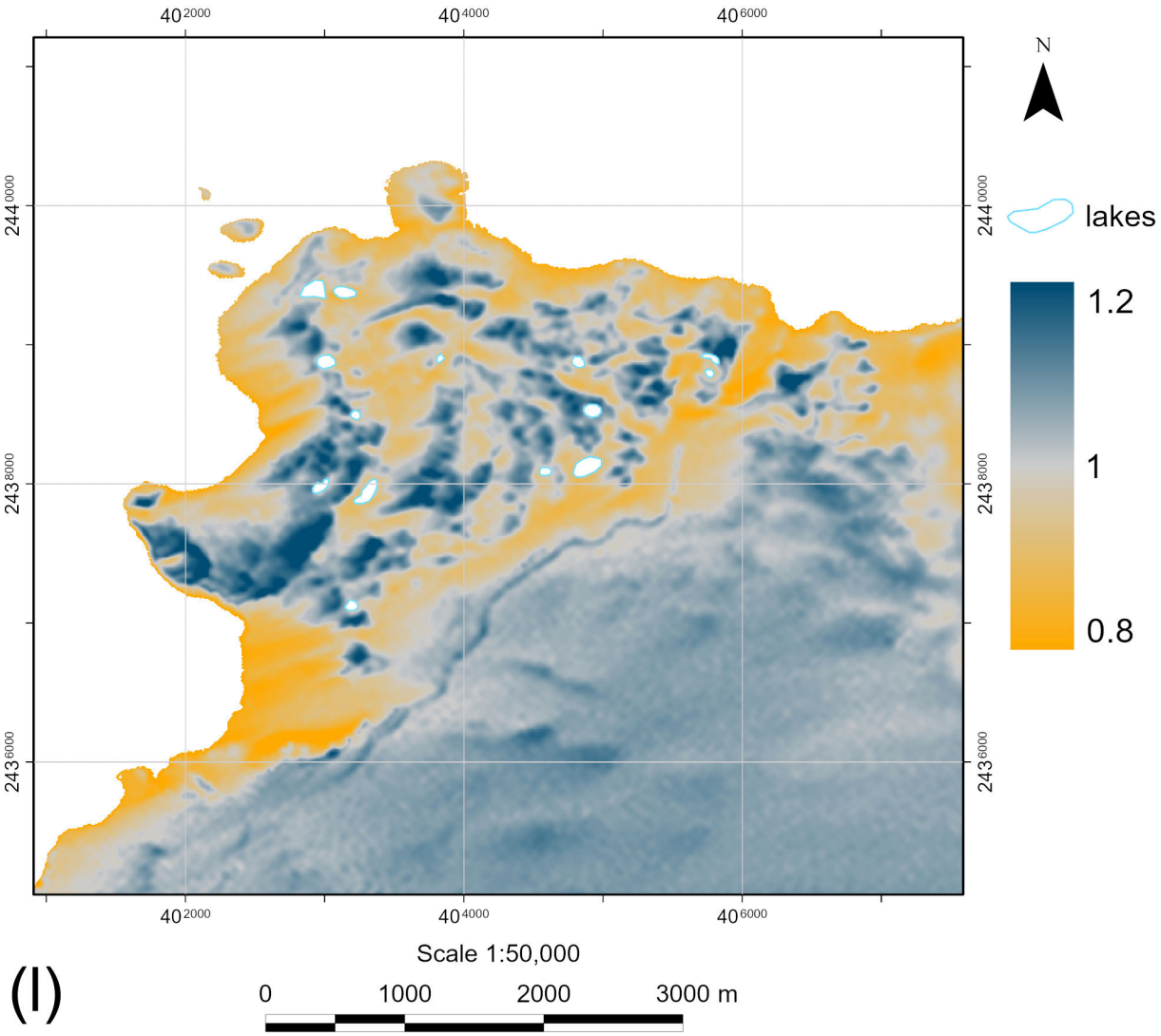

Fig. 3, cont'd Cape Hinode: (l) Wind exposition index.

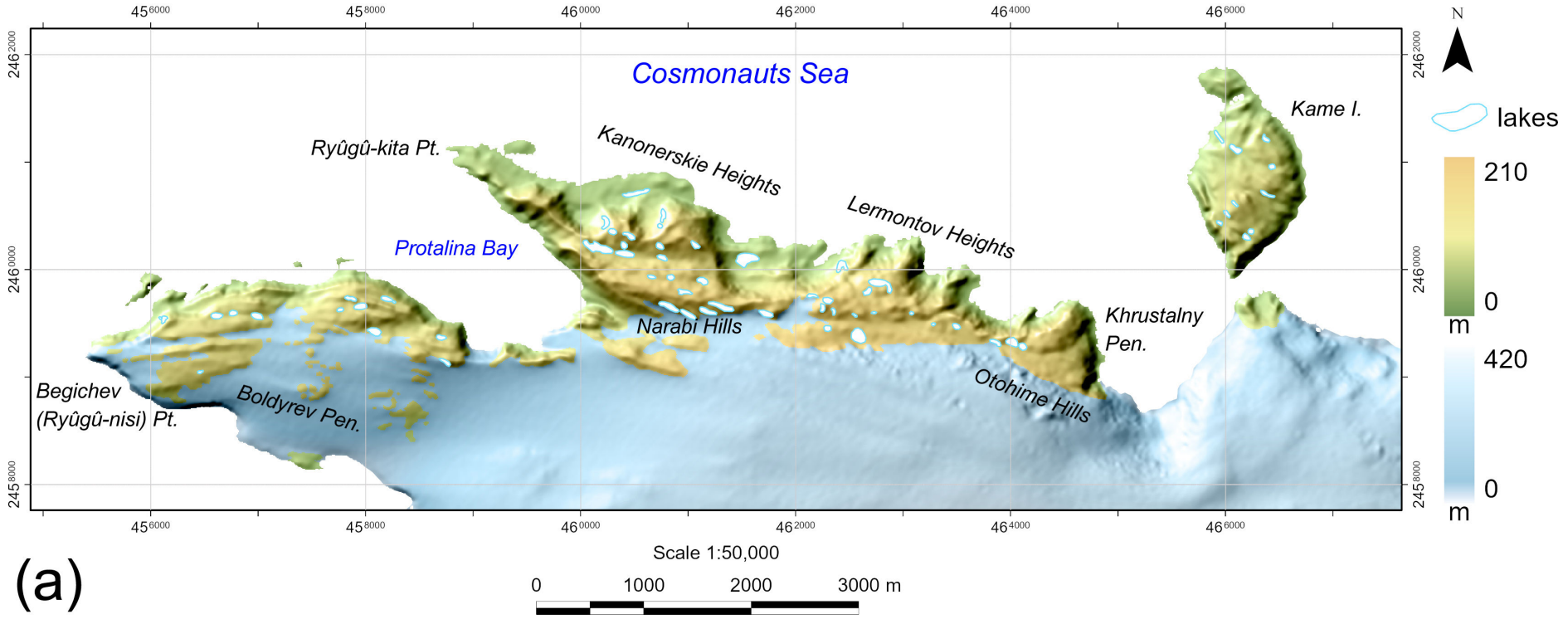

Fig. 4 Polkanov Hills (Cape Ryûgû): (a) Elevation.

(Continued)

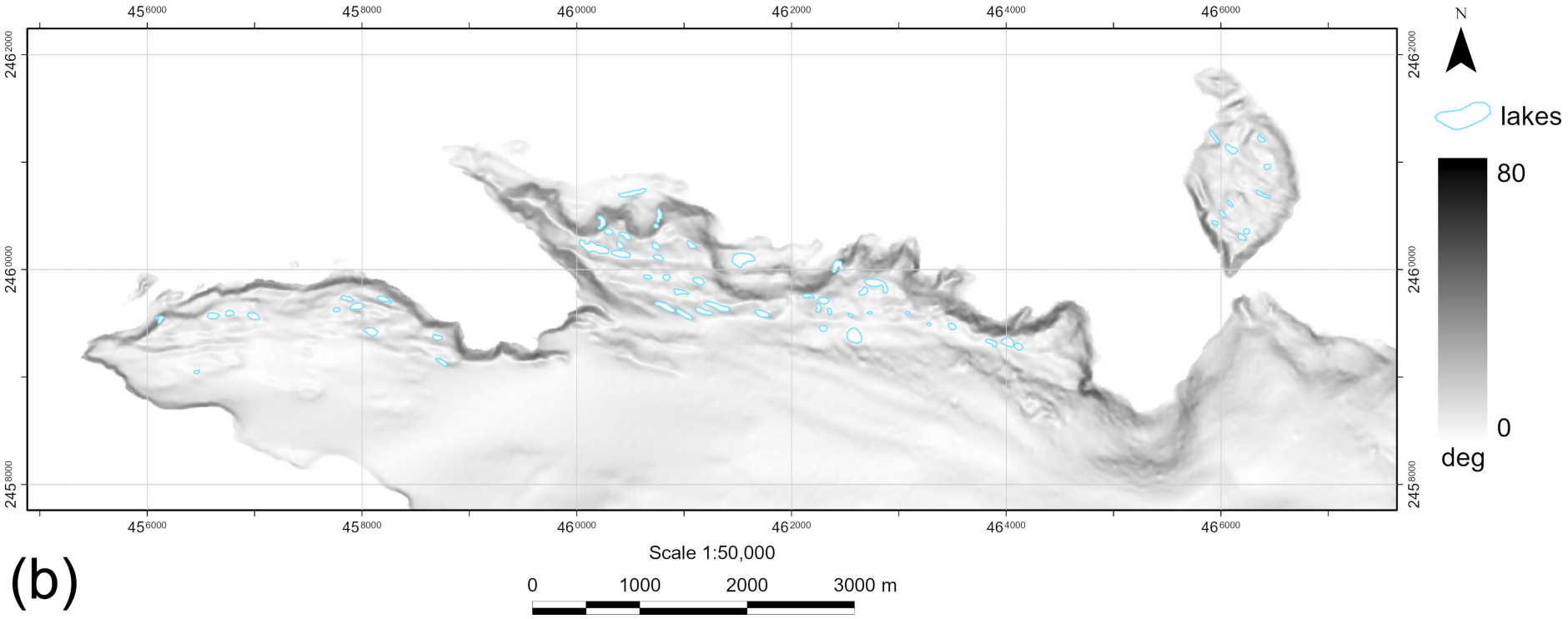

Fig. 4, cont'd Polkanov Hills (Cape Ryûgû): (b) Slope.

(Continued)

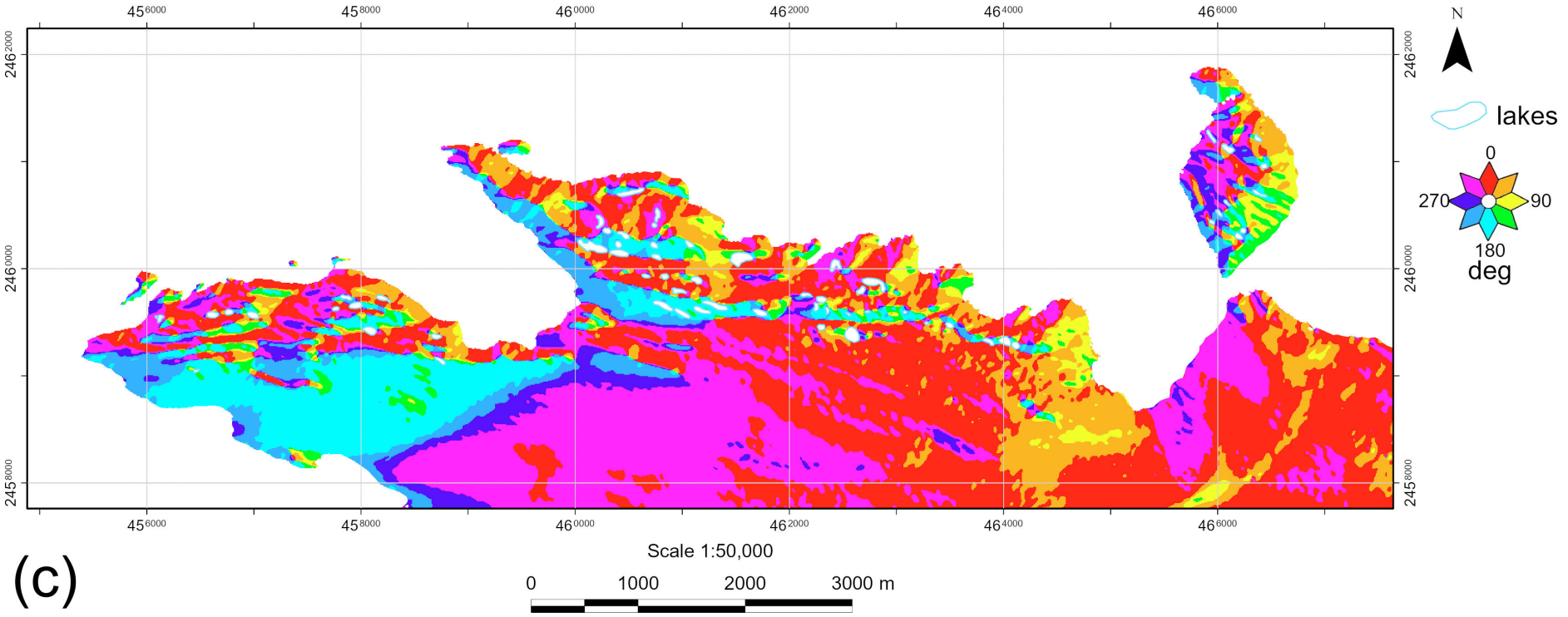

Fig. 4, cont'd Polkanov Hills (Cape Ryûgû): (c) Aspect.

(Continued)

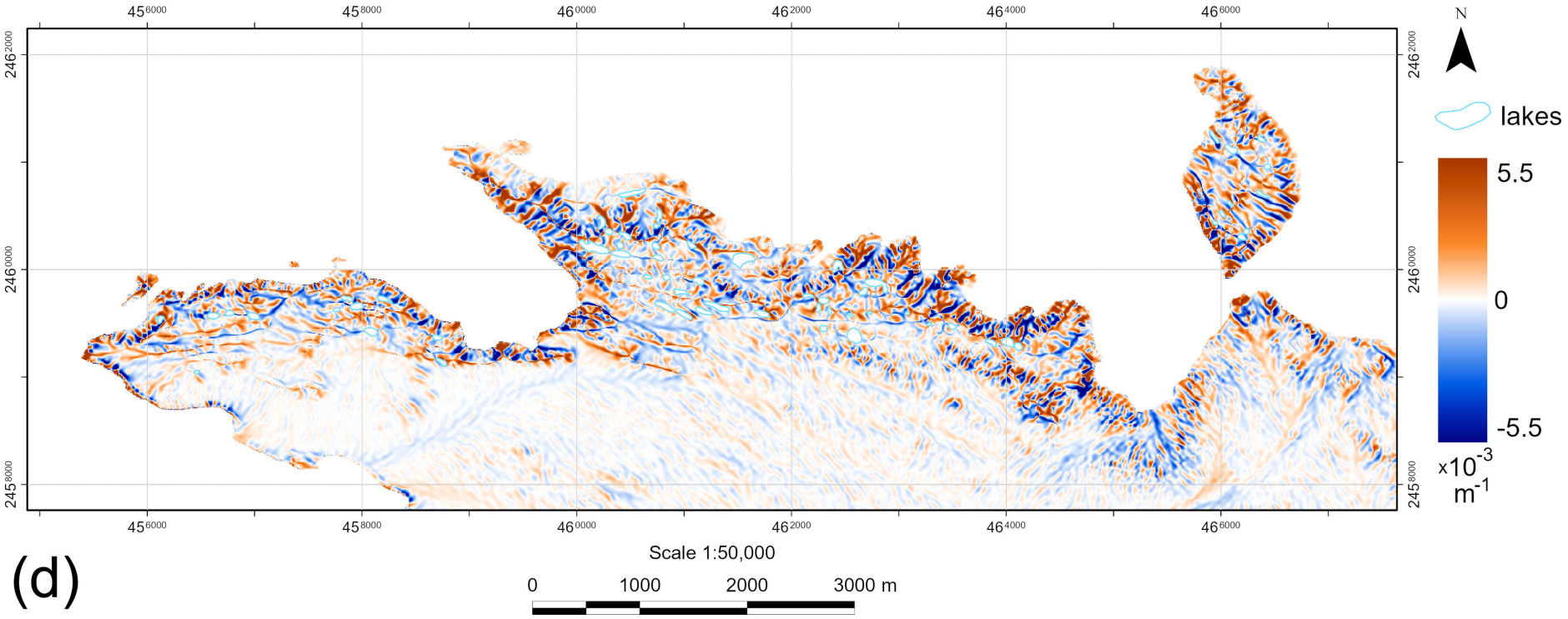

Fig. 4, cont'd Polkanov Hills (Cape Ryûgû): (d) Horizontal curvature.

(Continued)

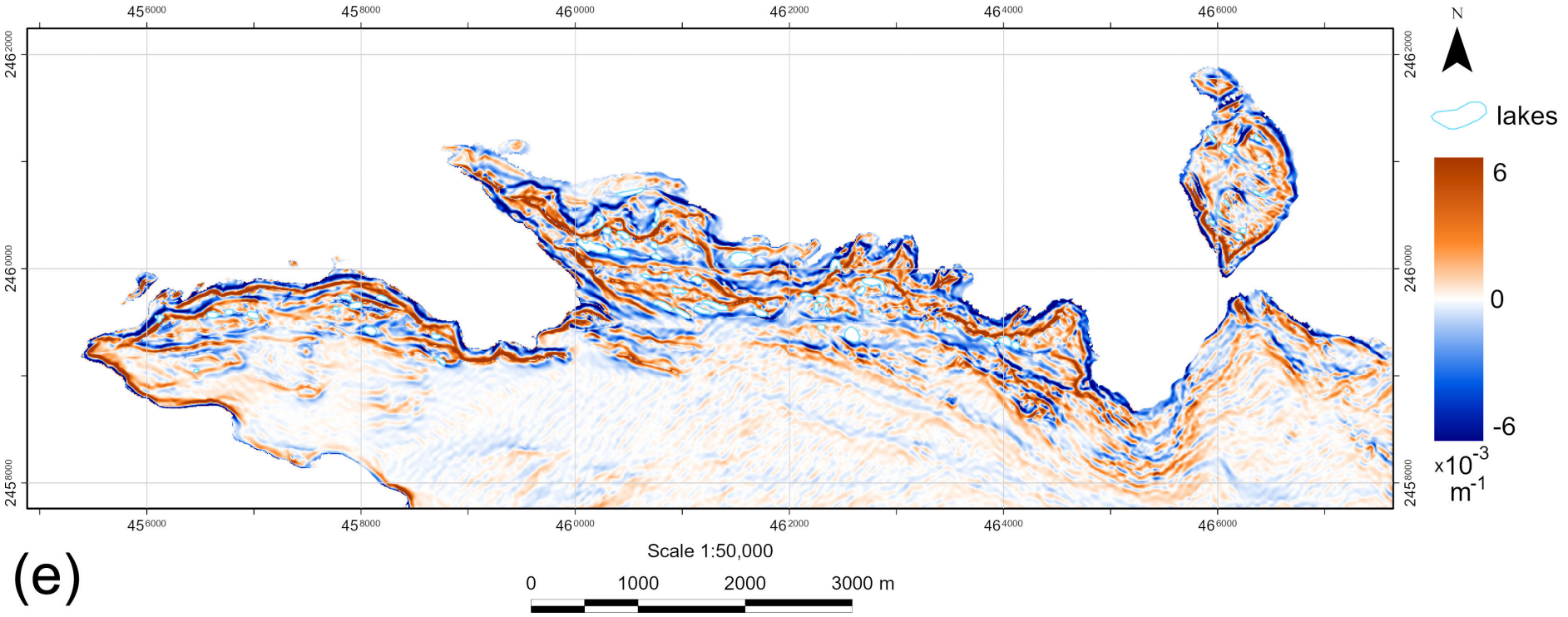

Fig. 4, cont'd Polkanov Hills (Cape Ryûgû): (e) Vertical curvature.

(Continued)

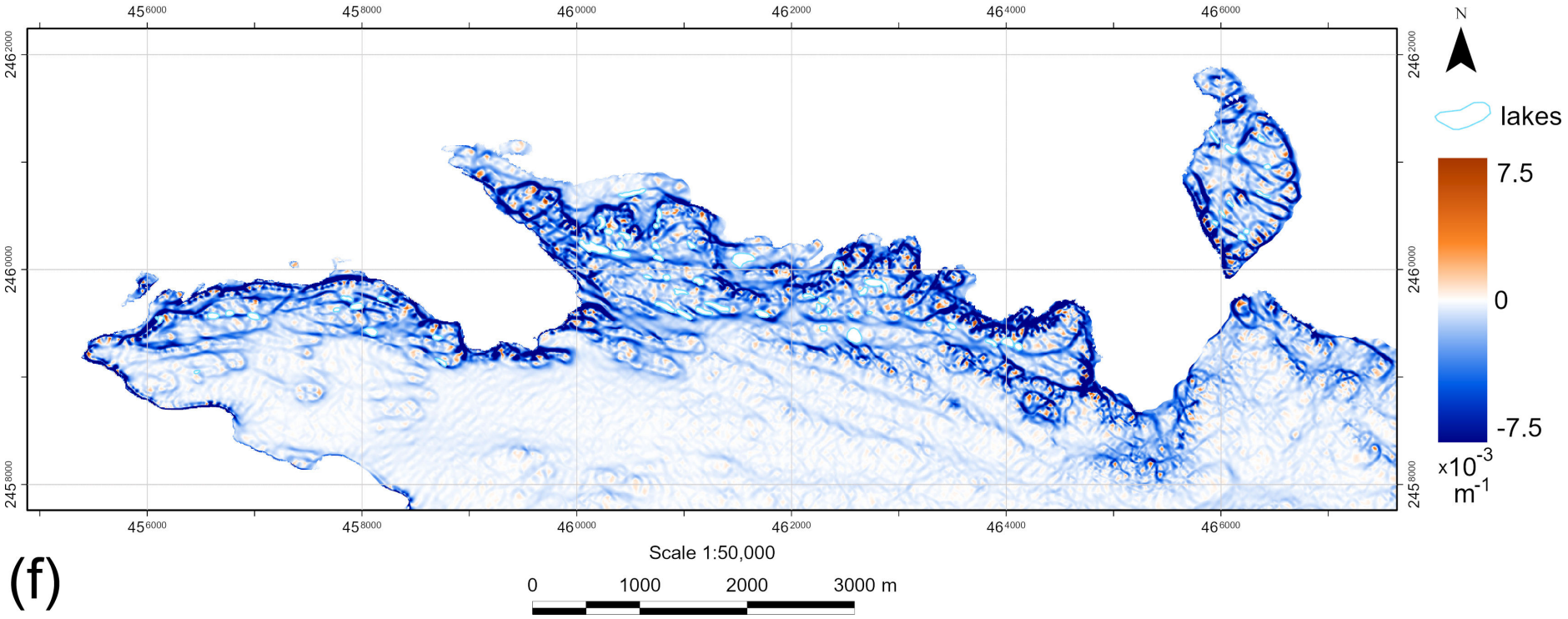

Fig. 4, cont'd Polkanov Hills (Cape Ryûgû): (f) Minimal curvature.

(Continued)

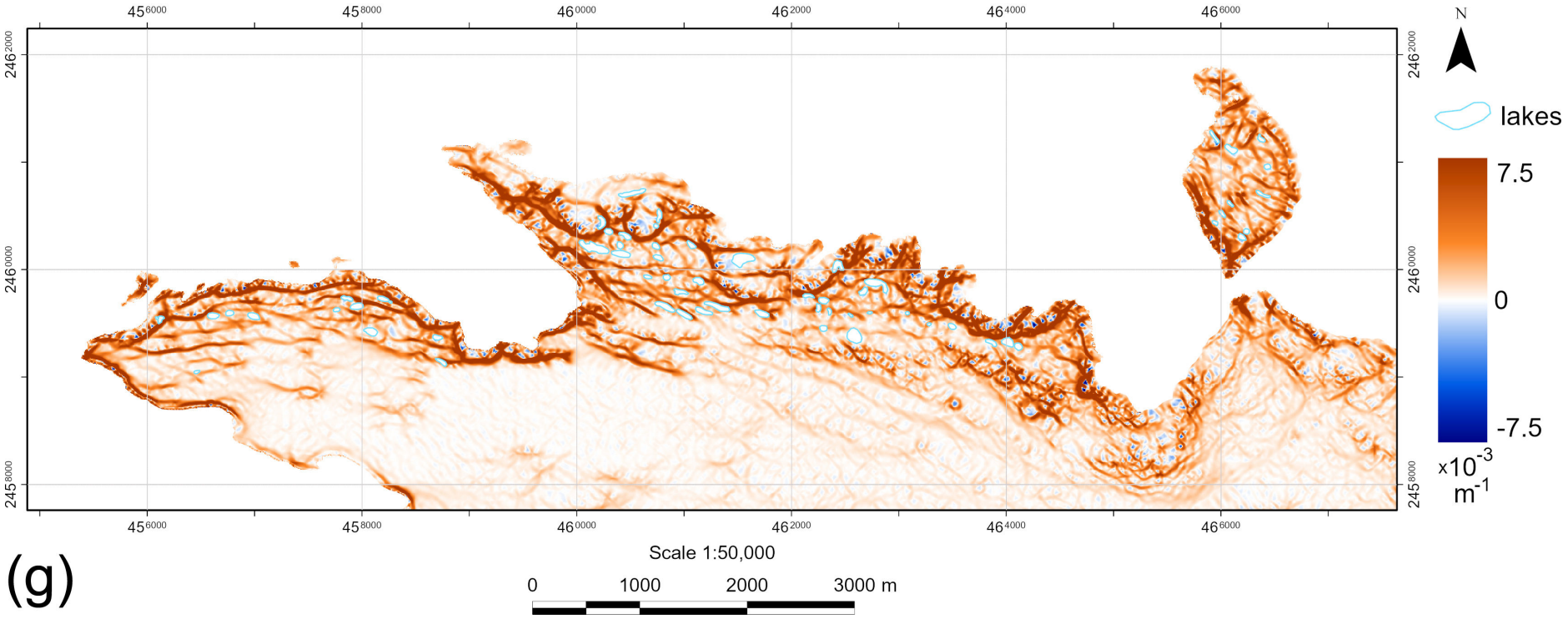

Fig. 4, cont'd Polkanov Hills (Cape Ryûgû): (g) Maximal curvature.

(Continued)

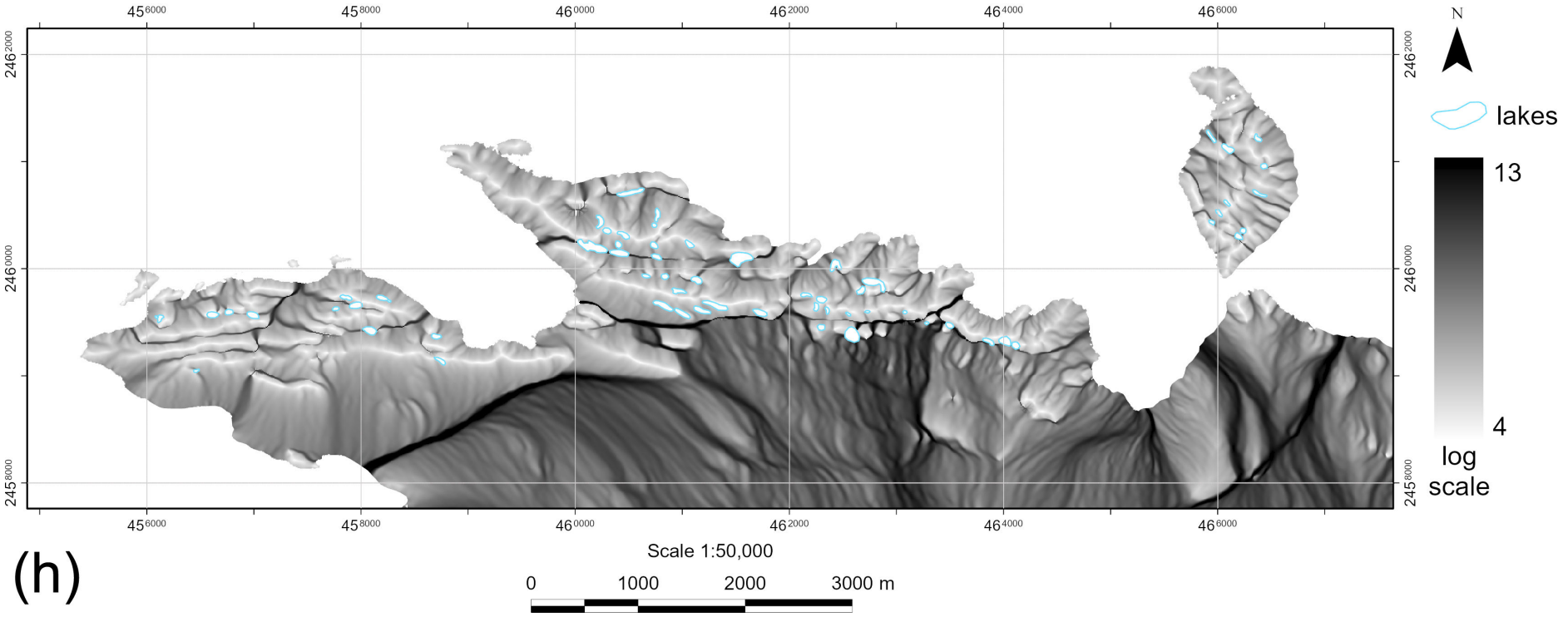

Fig. 4, cont'd Polkanov Hills (Cape Ryûgû): (h) Catchment area.

(Continued)

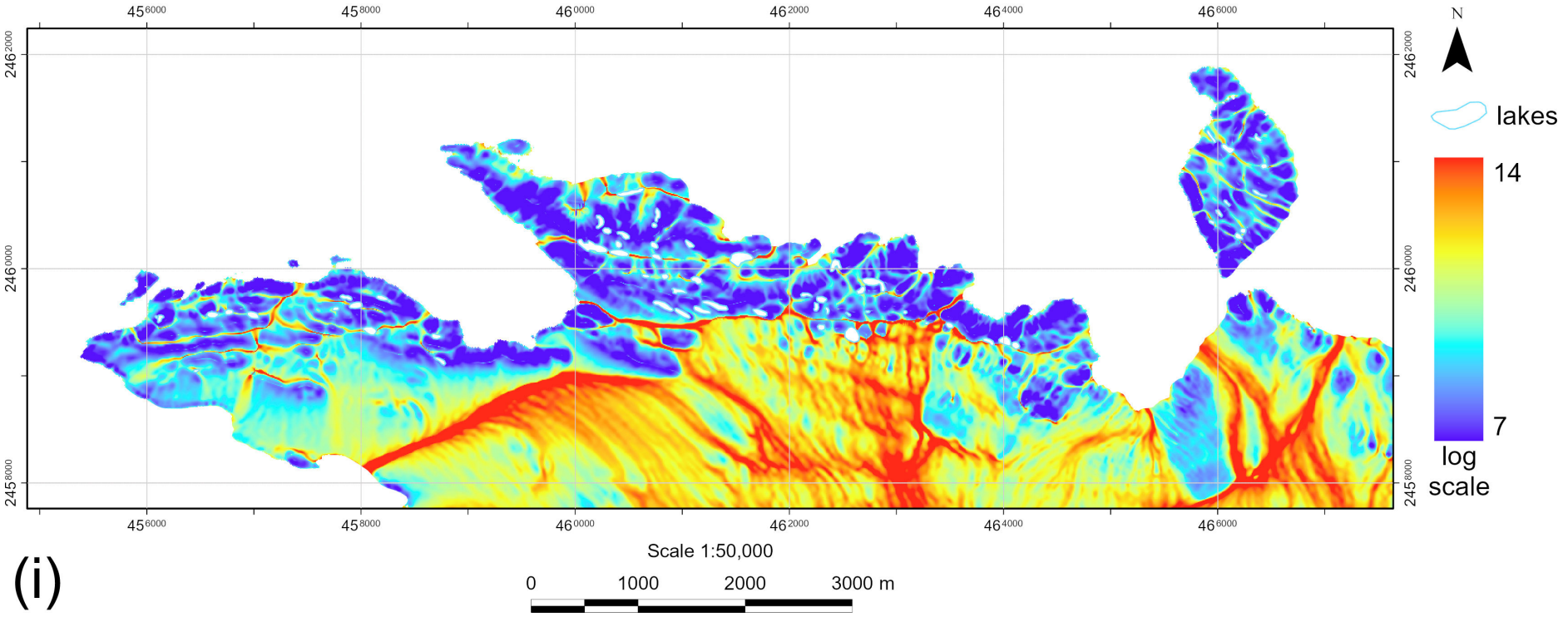

Fig. 4, cont'd Polkanov Hills (Cape Ryûgû): (i) Topographic wetness index.

(Continued)

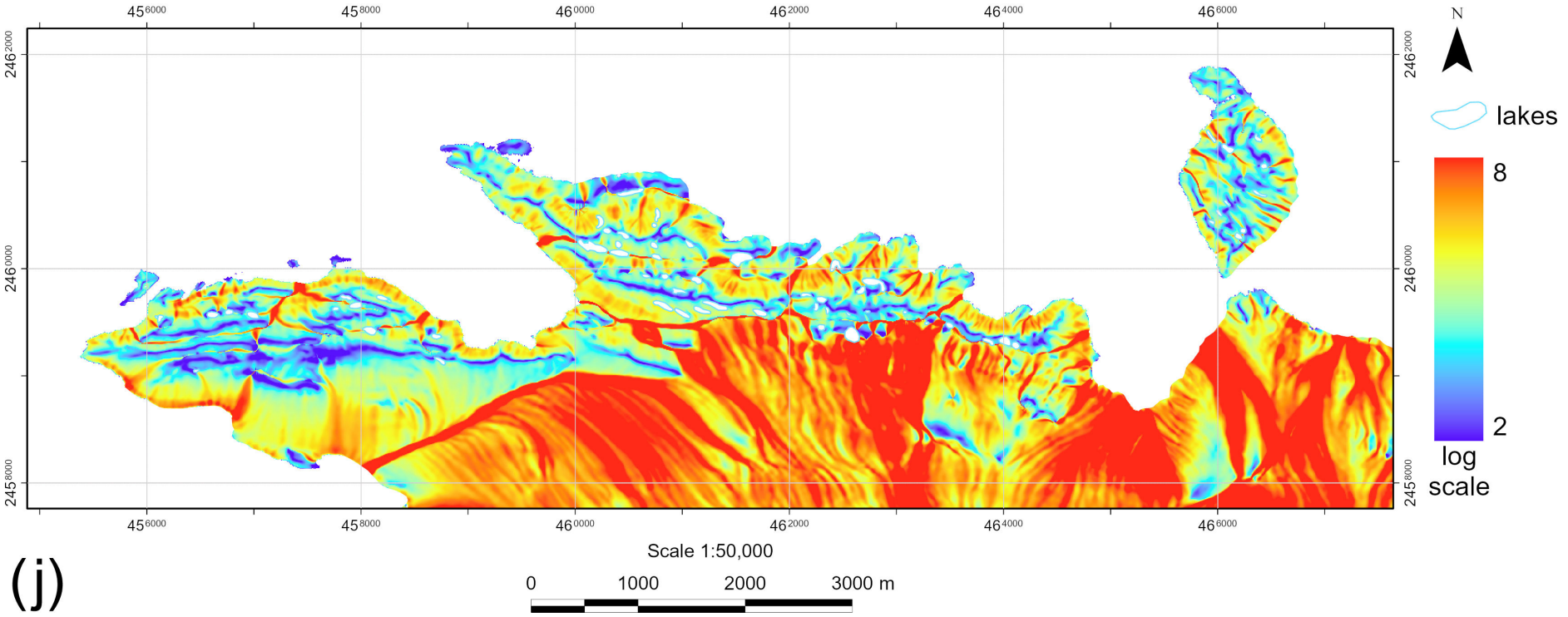

Fig. 4, cont'd Polkanov Hills (Cape Ryûgû): (j) Stream power index.

(Continued)

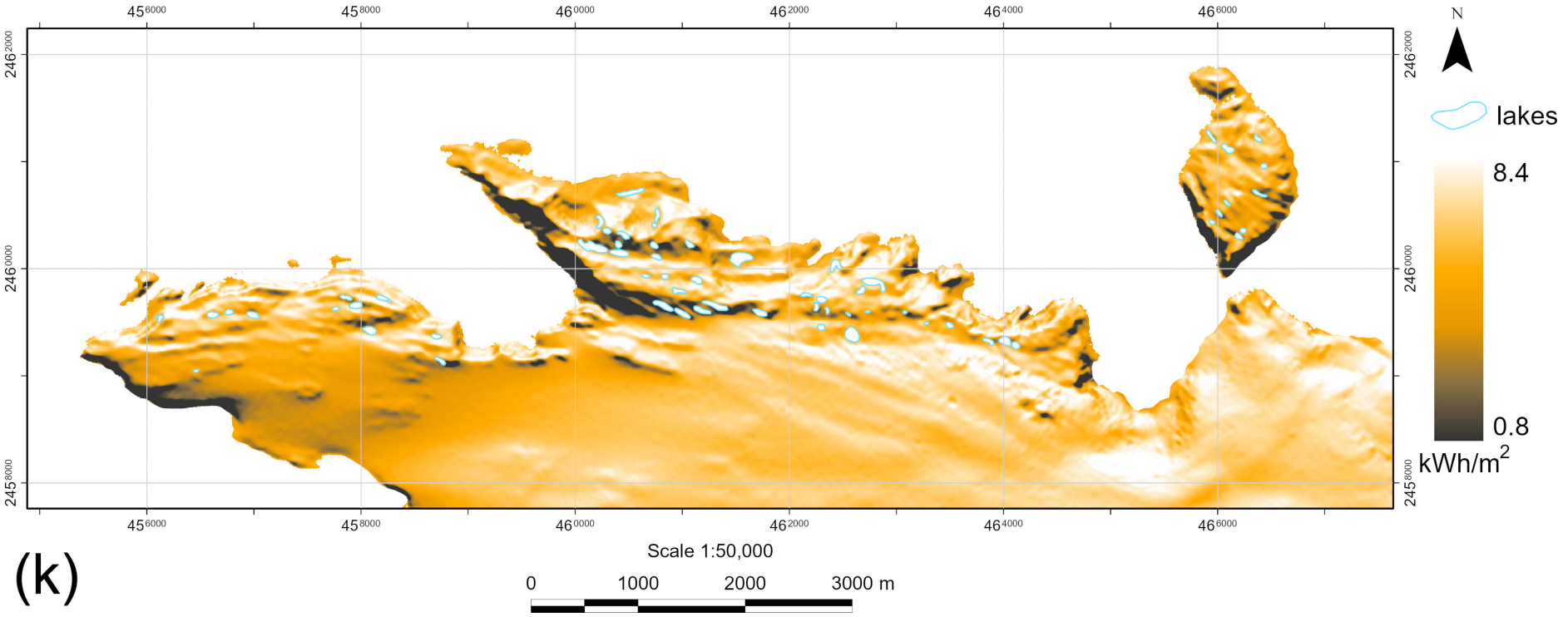

Fig. 4, cont'd Polkanov Hills (Cape Ryûgû): (k) Total insolation.

(Continued)

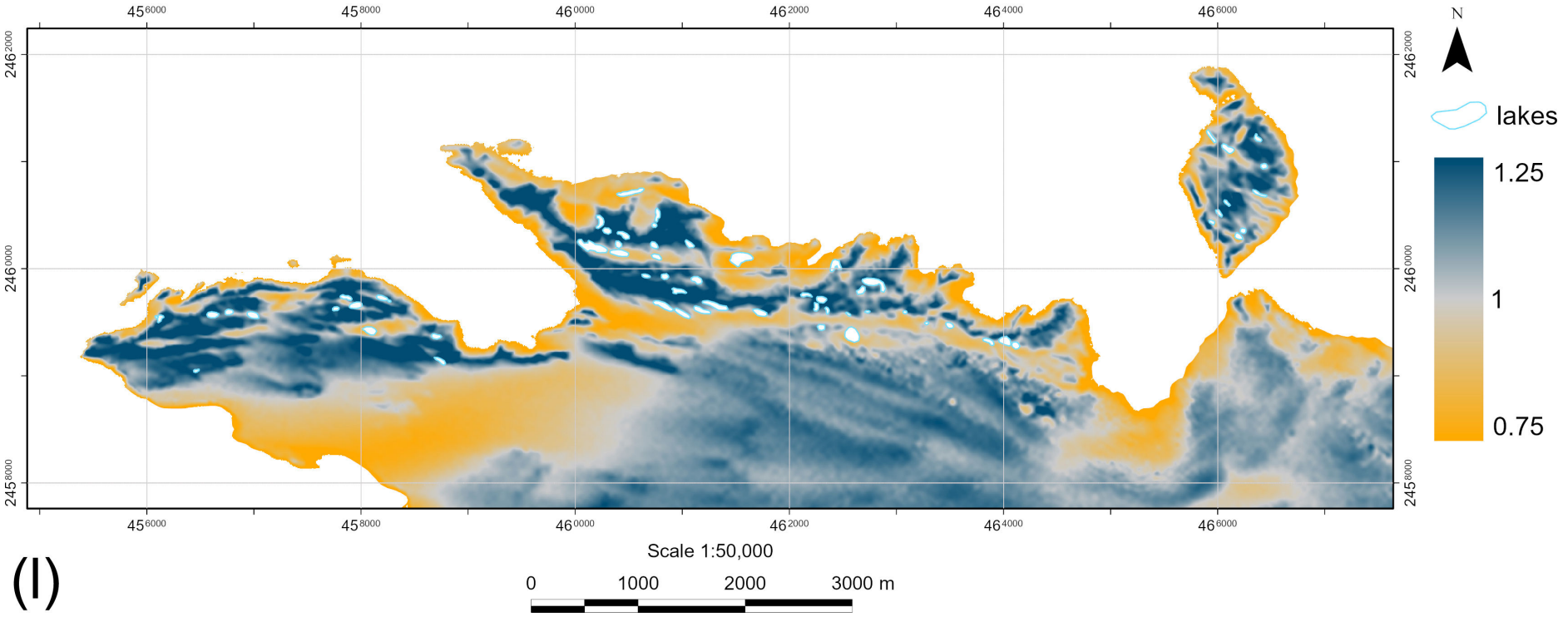

Fig. 4, cont'd Polkanov Hills (Cape Ryûgû): (l) Wind exposition index.

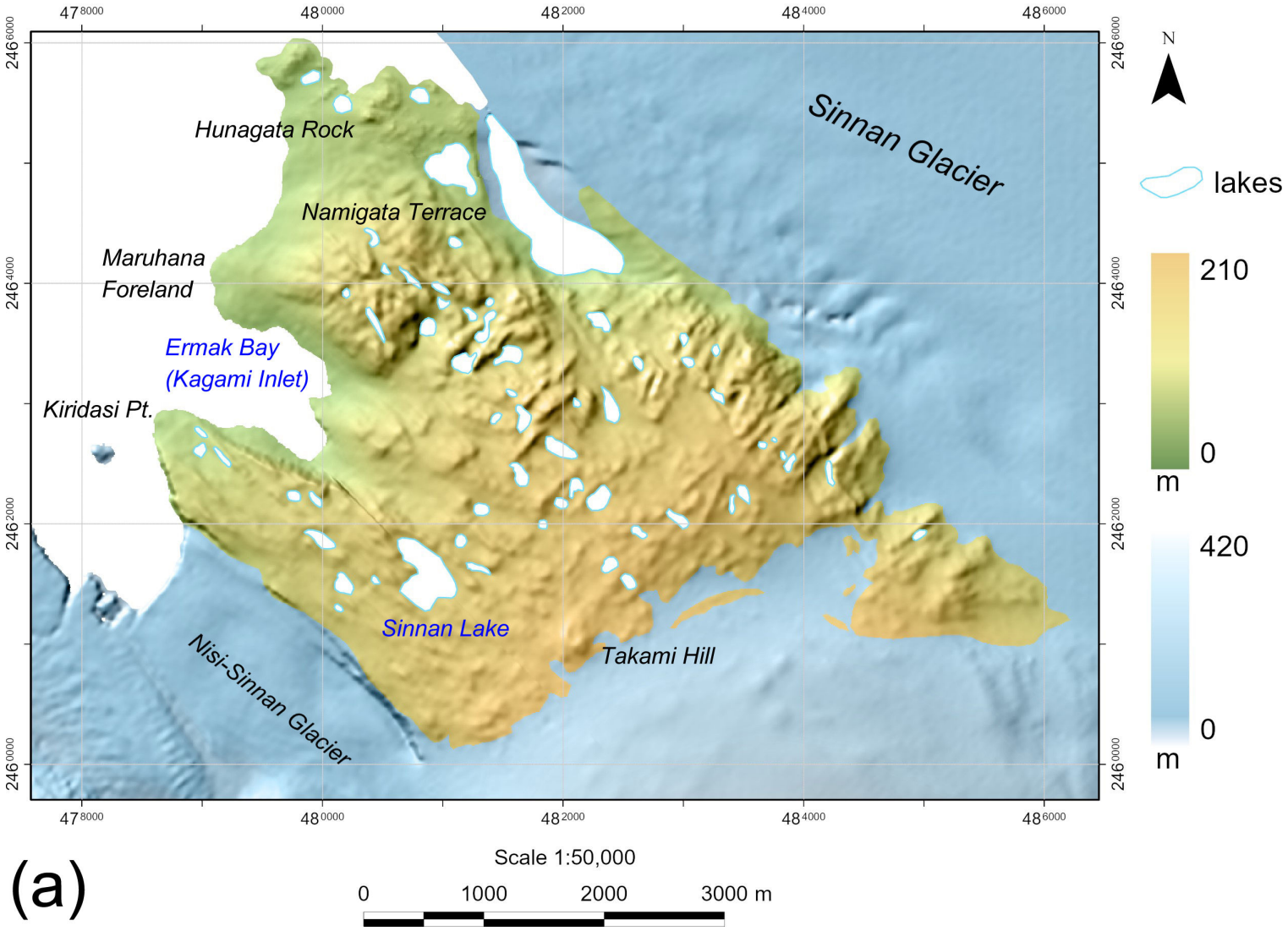

Fig. 5 Tereshkova Oasis (Sinnan Rocks): (a) Elevation.

(Continued)

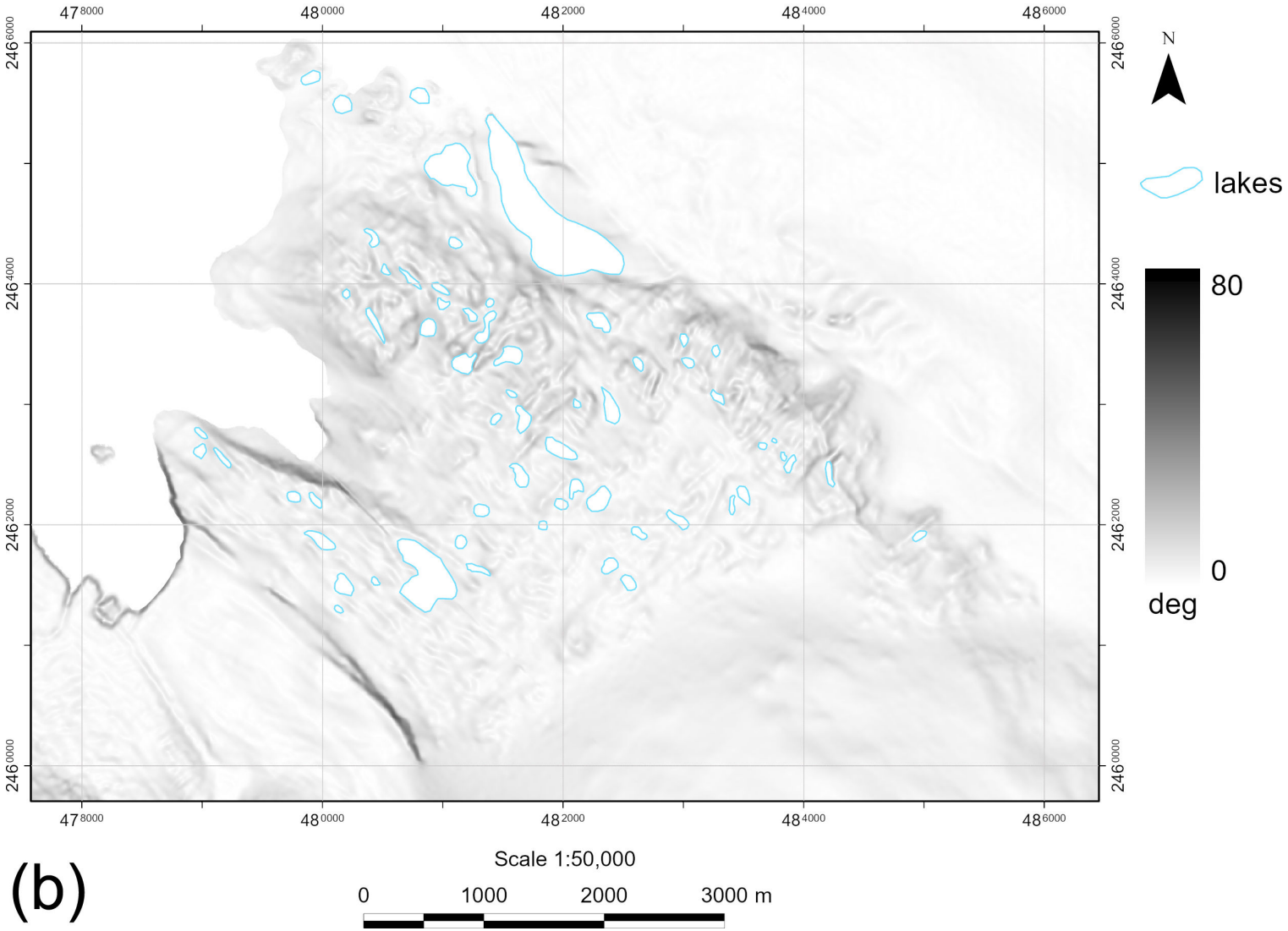

Fig. 5, cont'd Tereshkova Oasis (Sinnan Rocks): (b) Slope.

(Continued)

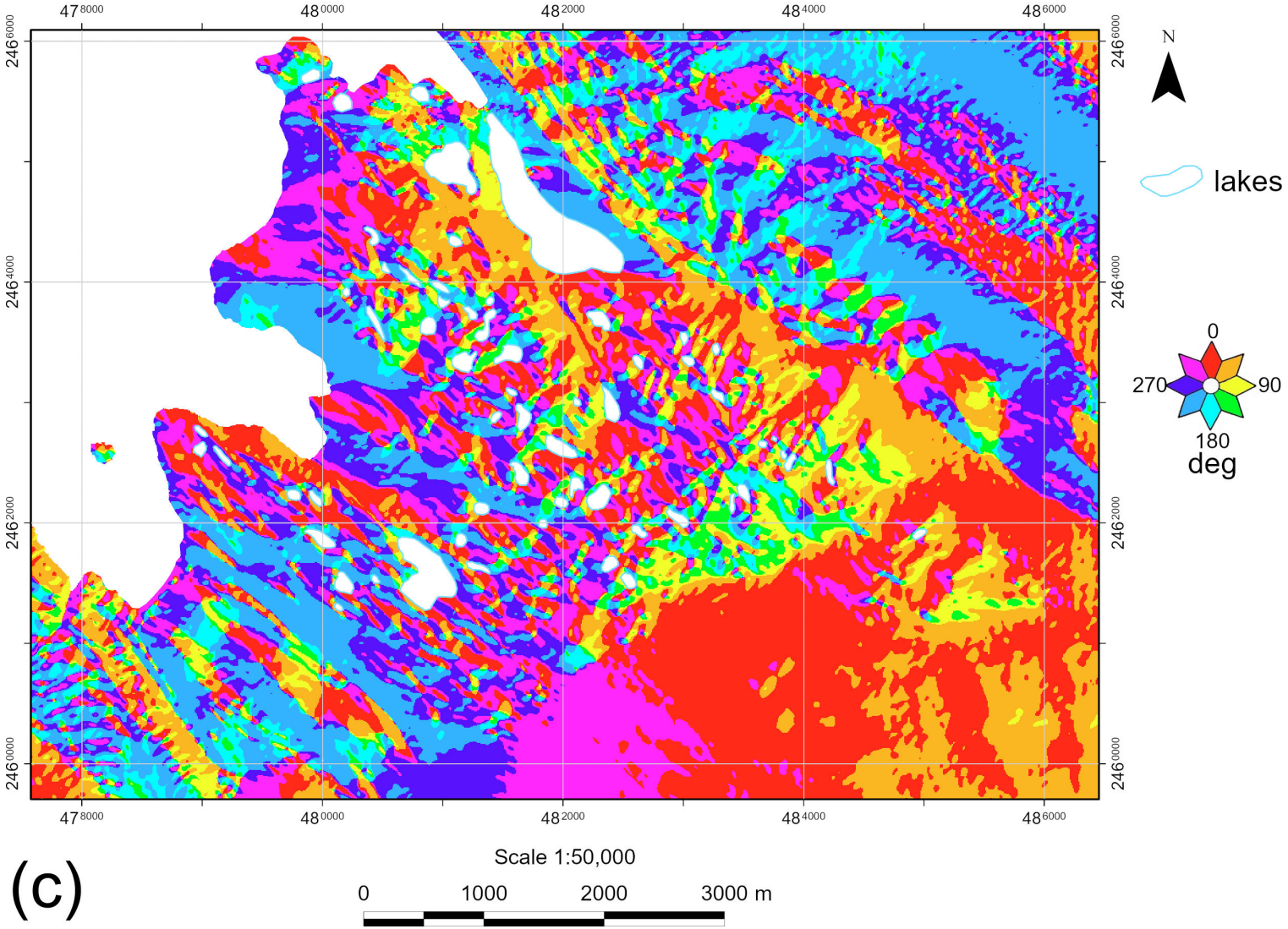

Fig. 5, cont'd Tereshkova Oasis (Sinnan Rocks): (c) Aspect.

(Continued)

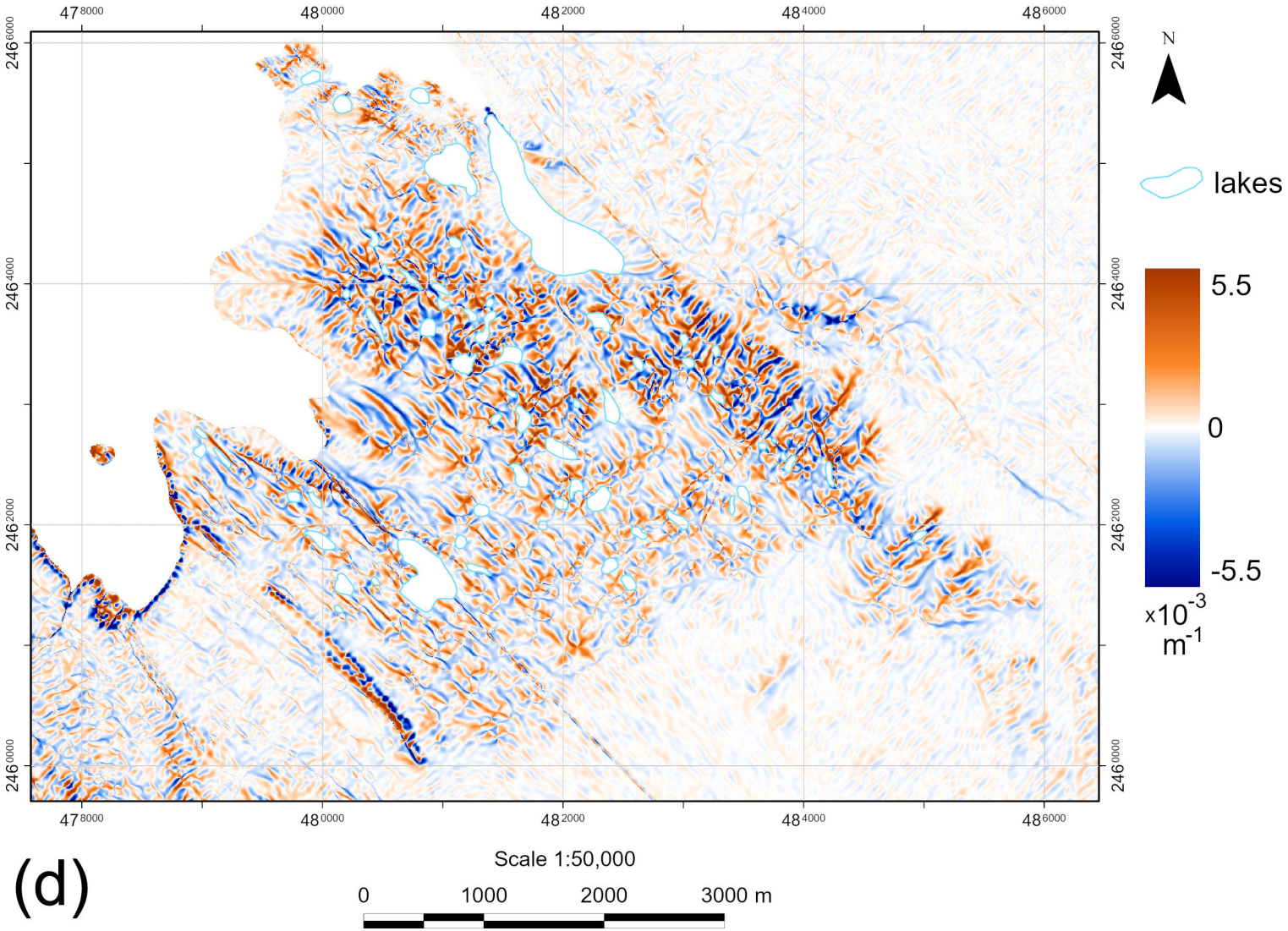

Fig. 5, cont'd Tereshkova Oasis (Sinnan Rocks): (d) Horizontal curvature.

(Continued)

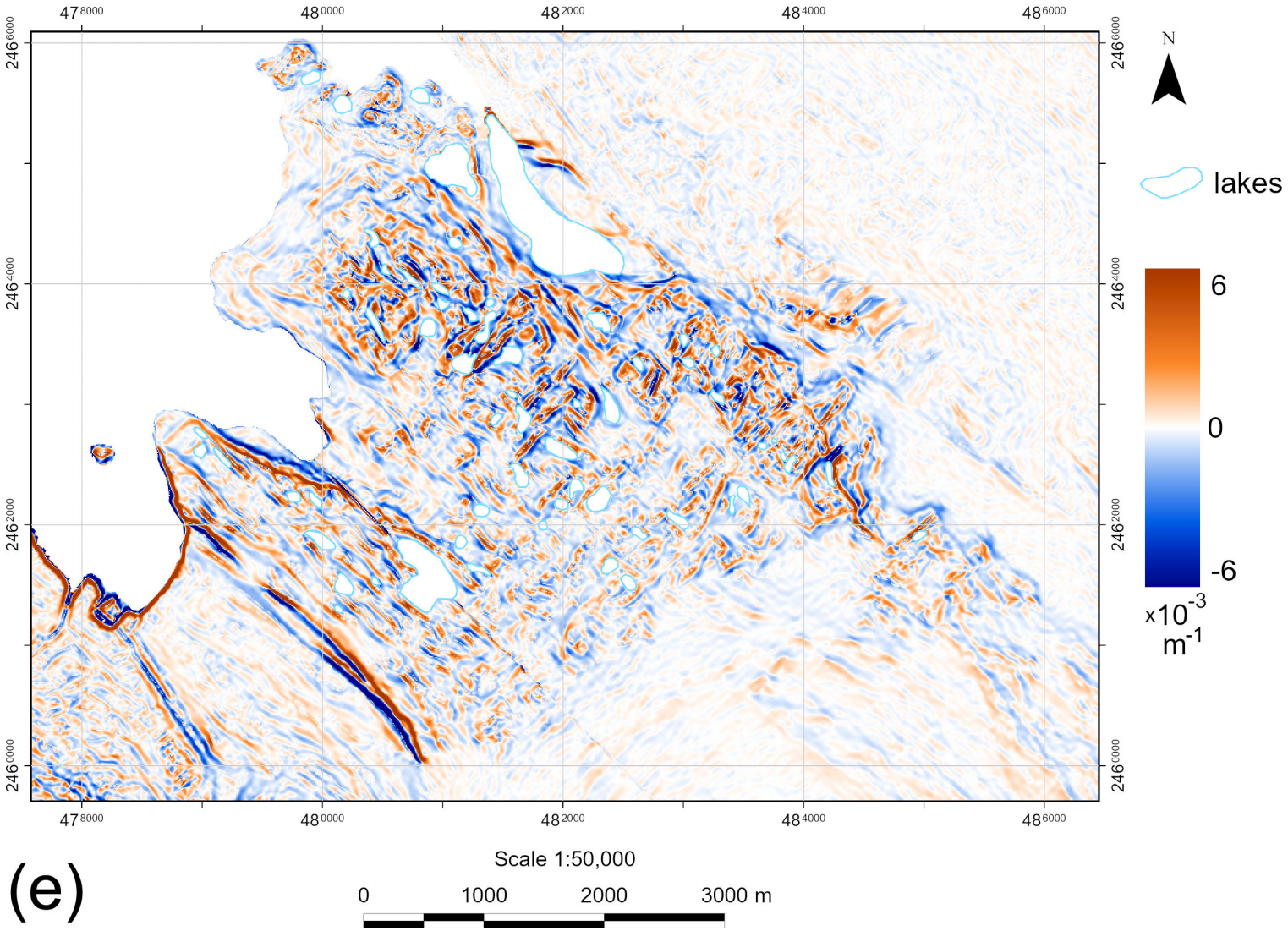

Fig. 5, cont'd Tereshkova Oasis (Sinnan Rocks): (e) Vertical curvature.

(Continued)

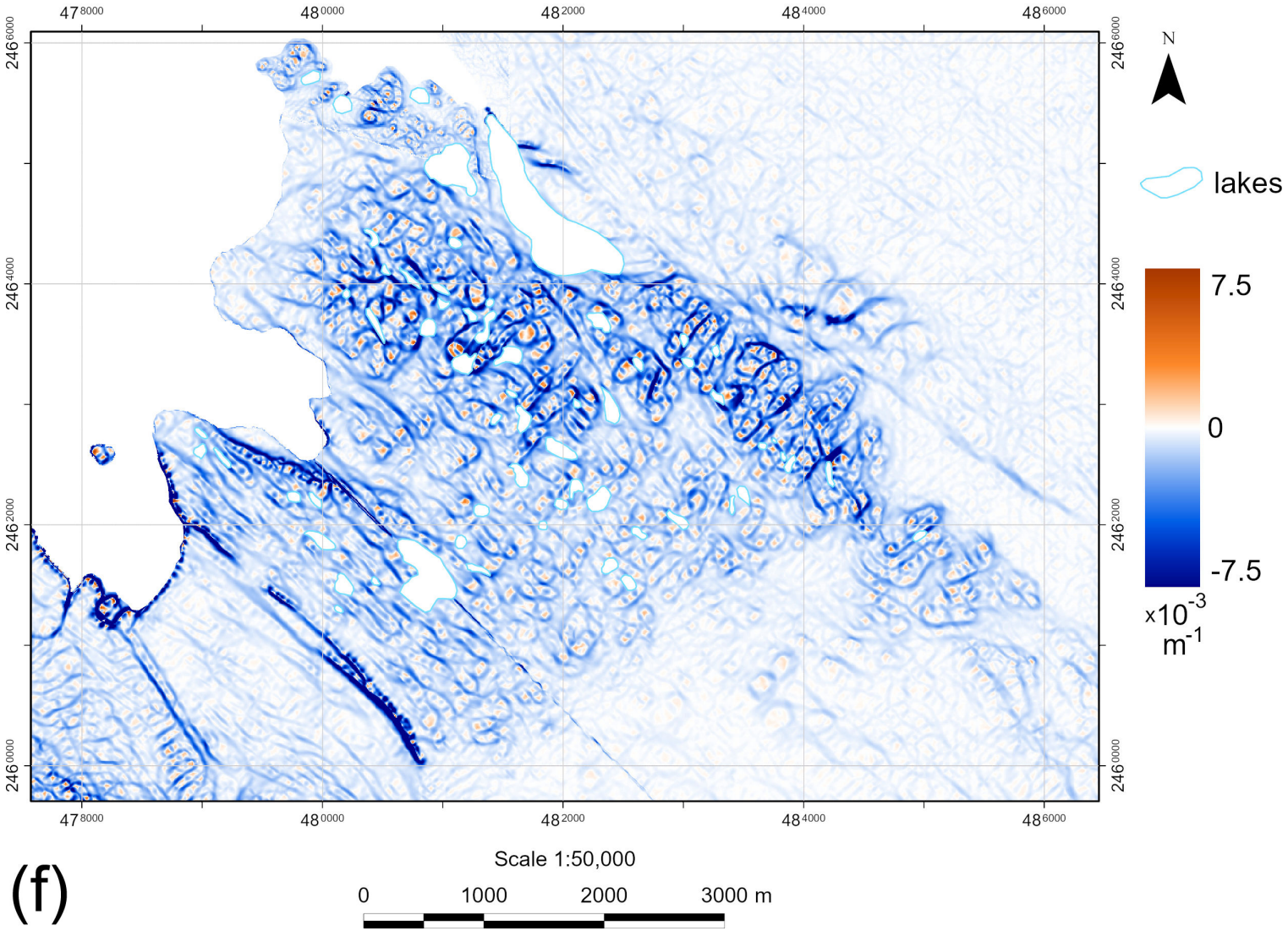

Fig. 5, cont'd Tereshkova Oasis (Sinnan Rocks): (f) Minimal curvature.

(Continued)

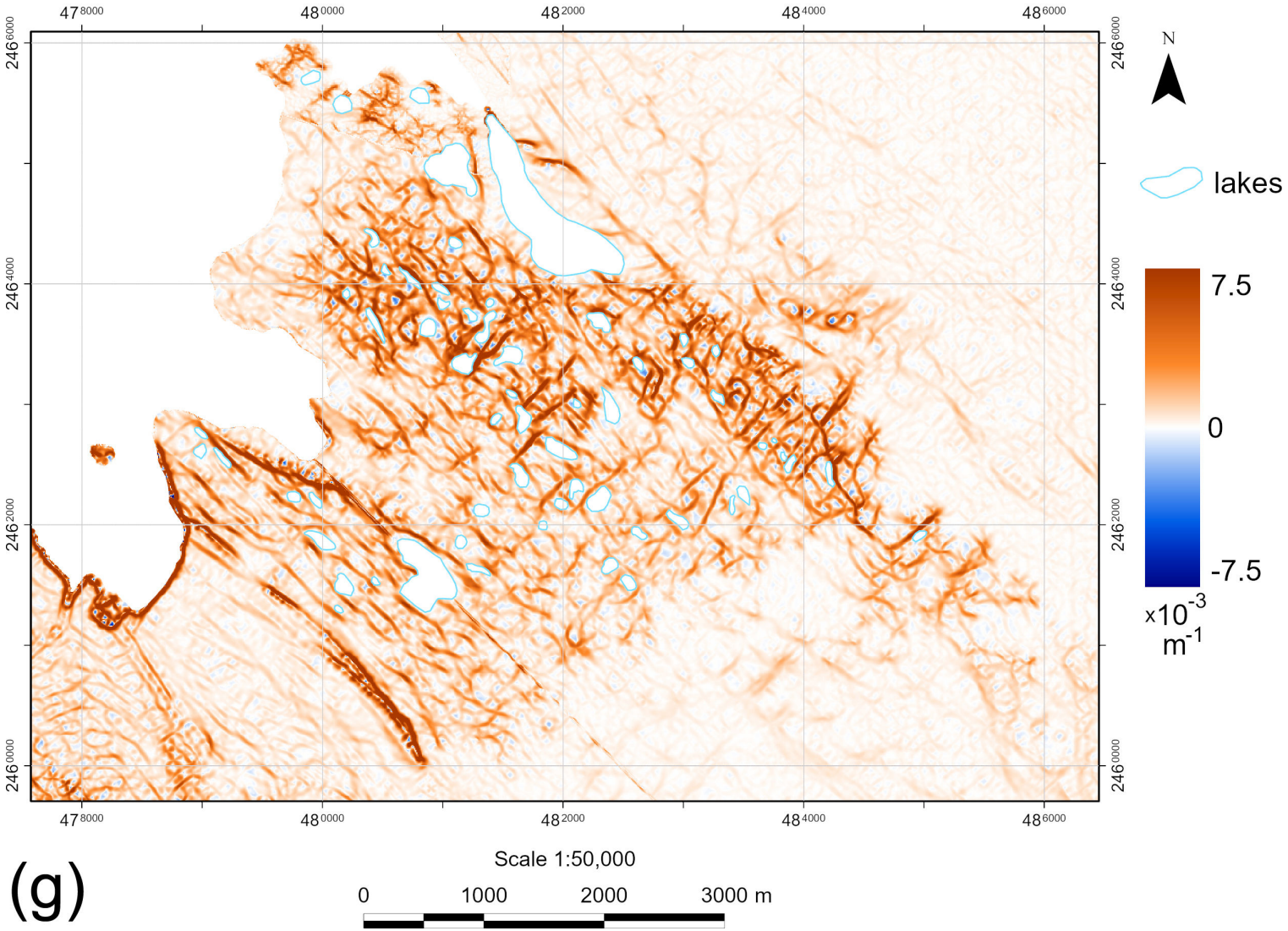

Fig. 5, cont'd Tereshkova Oasis (Sinnan Rocks): (g) Maximal curvature.

(Continued)

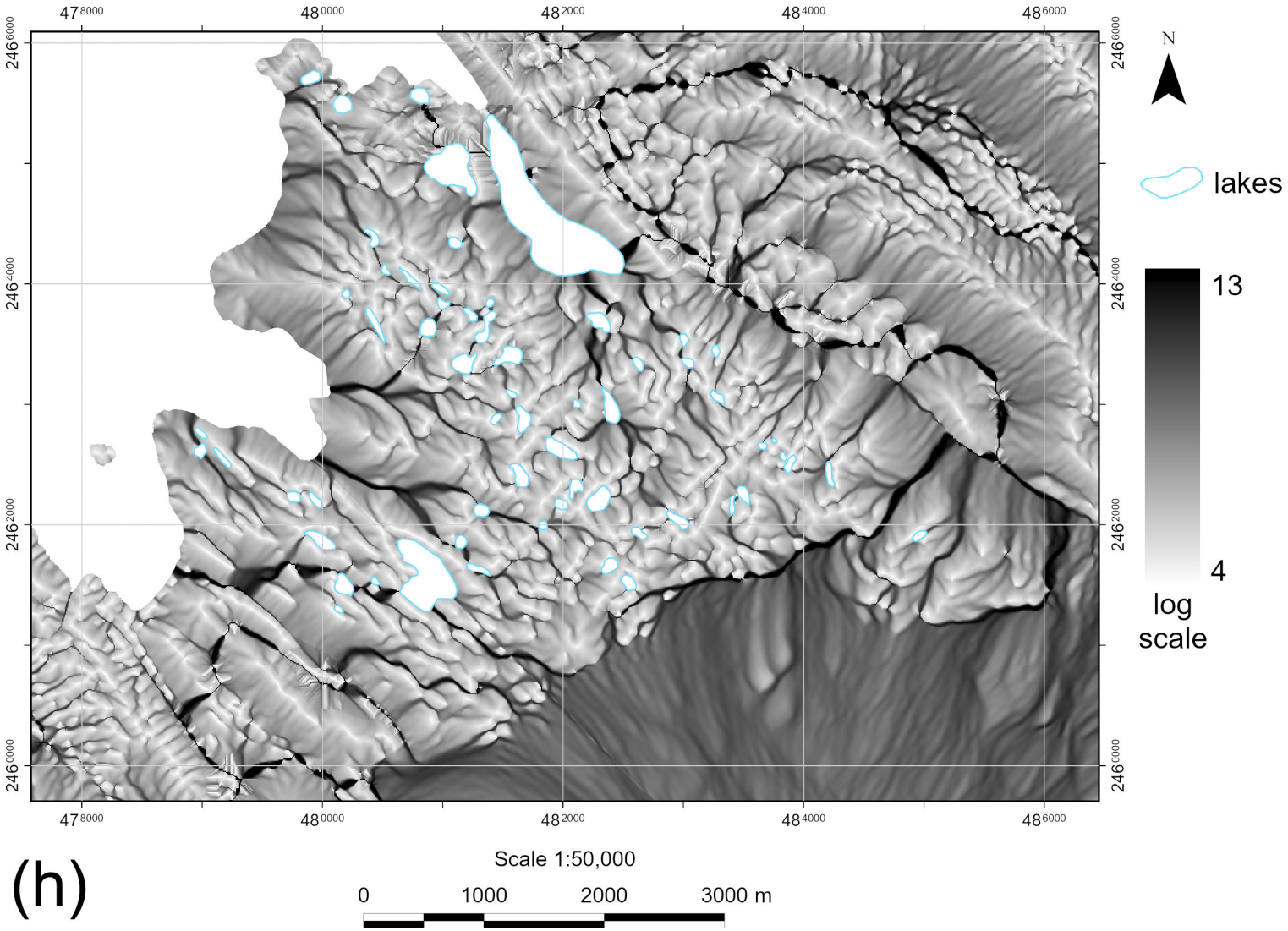

Fig. 5, cont'd Tereshkova Oasis (Sinnan Rocks): (h) Catchment area.

(Continued)

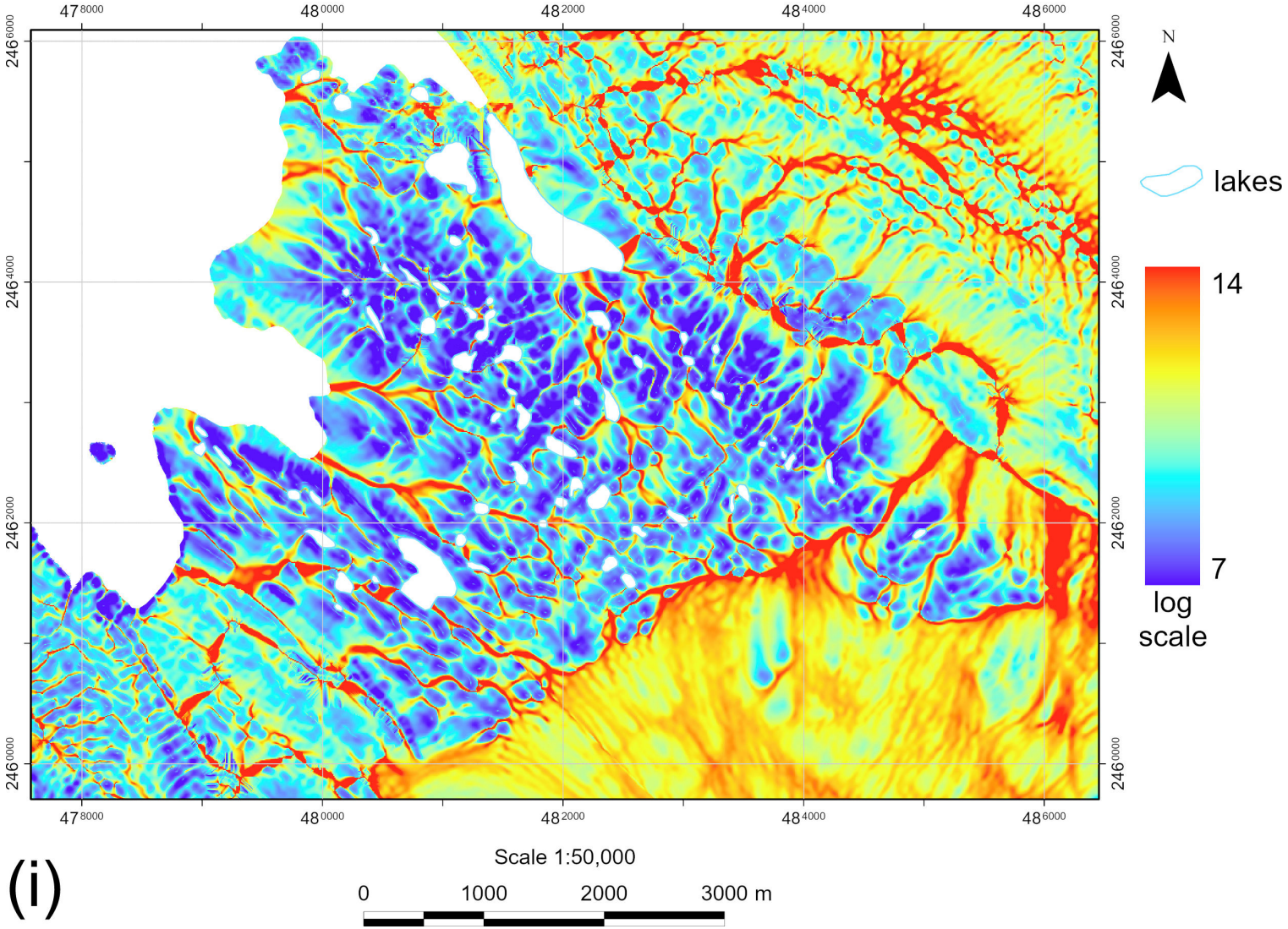

Fig. 5, cont'd Tereshkova Oasis (Sinnan Rocks): (i) Topographic wetness index.

(Continued)

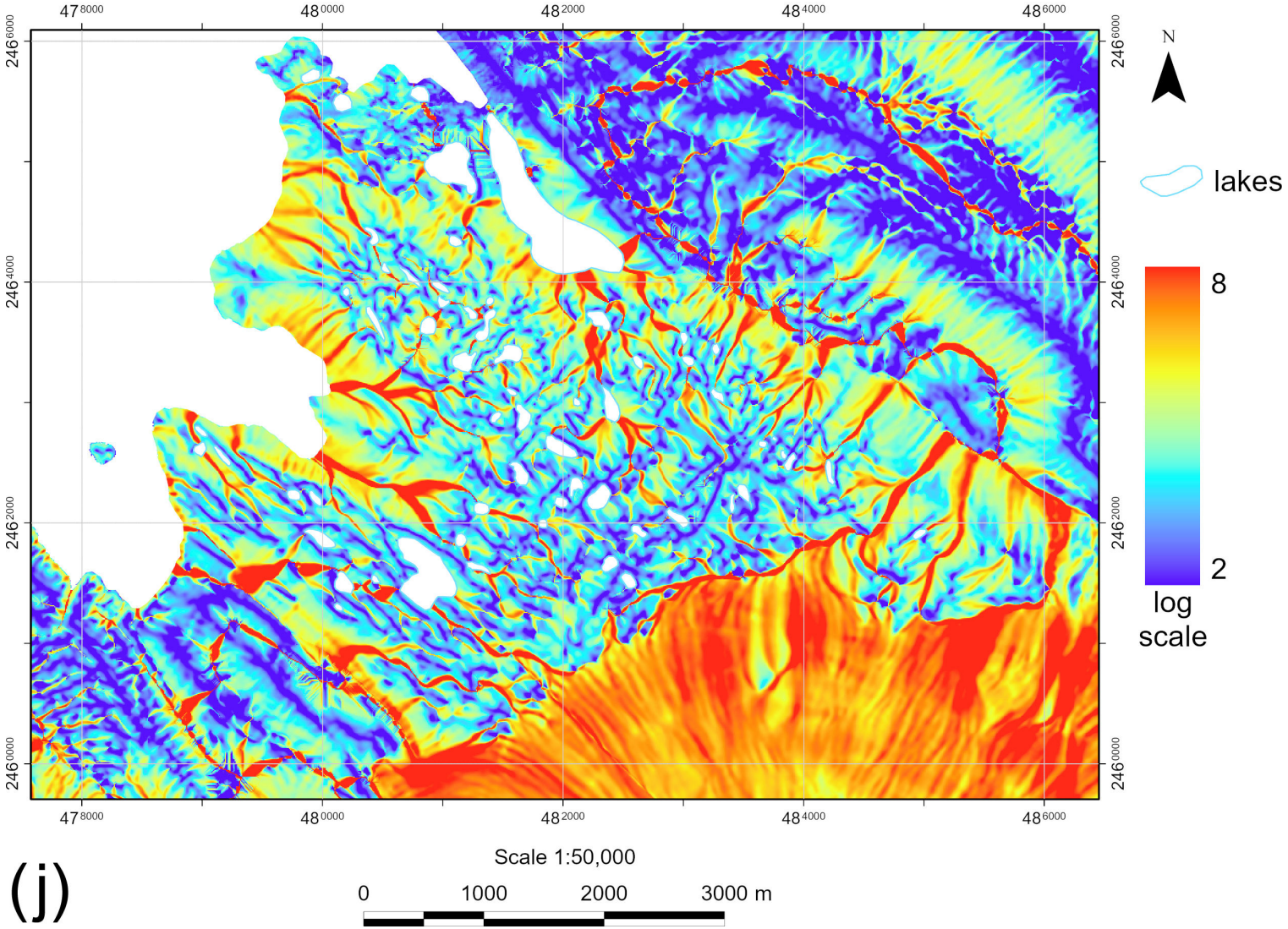

Fig. 5, cont'd Tereshkova Oasis (Sinnan Rocks): (j) Stream power index.

(Continued)

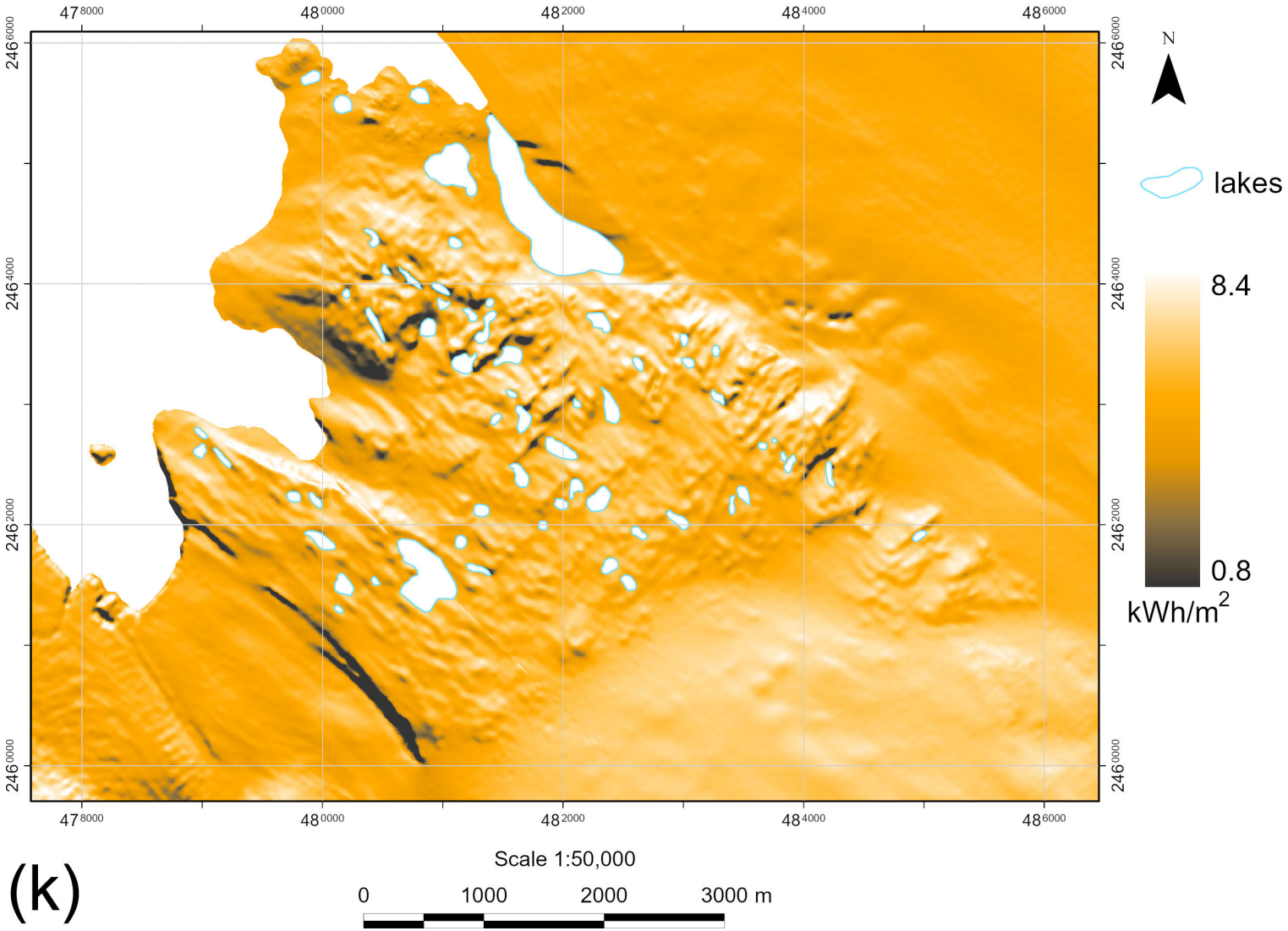

Fig. 5, cont'd Tereshkova Oasis (Sinnan Rocks): (k) Total insolation.

(Continued)

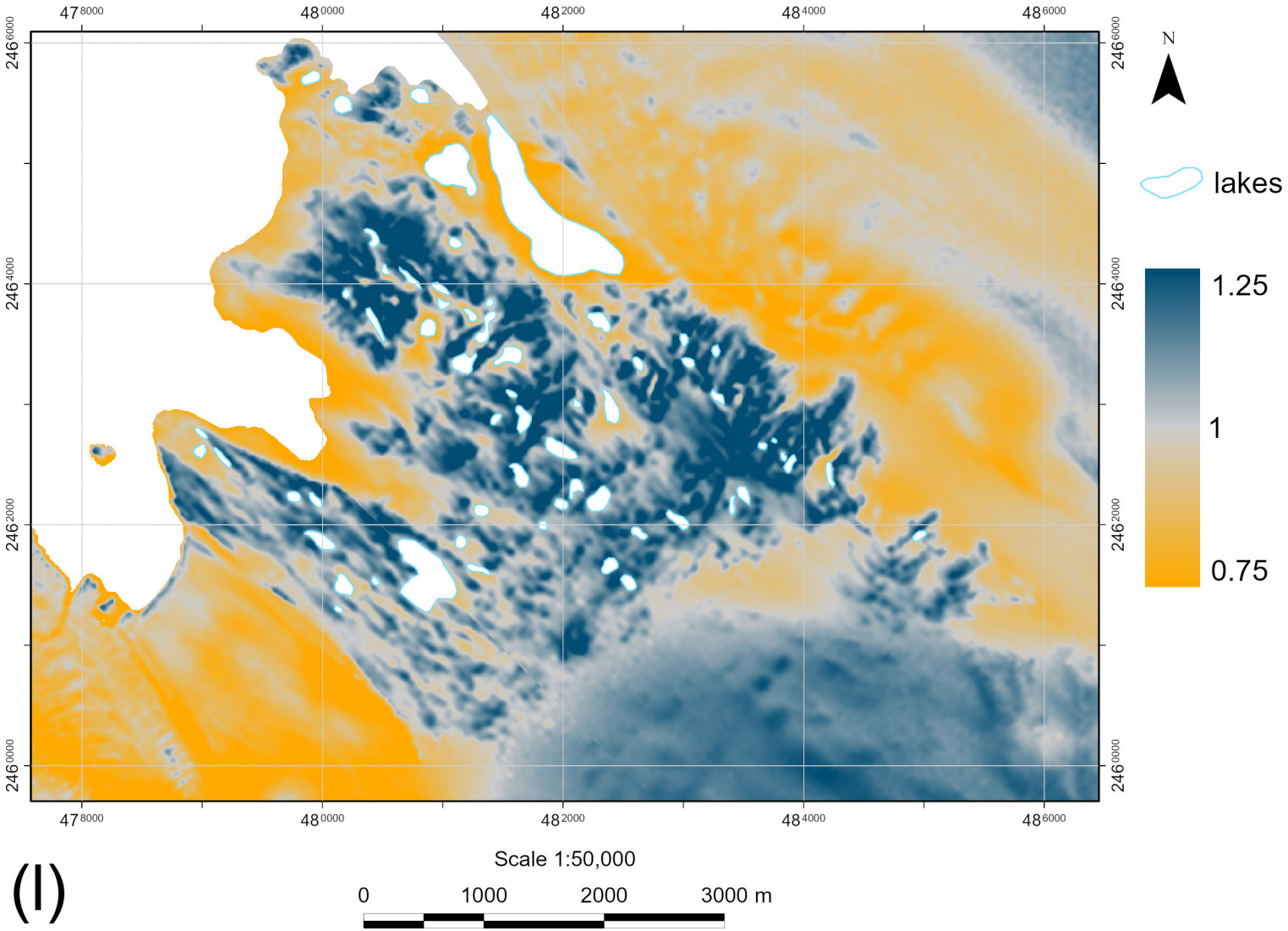

Fig. 5, cont'd Tereshkova Oasis (Sinnan Rocks): (l) Wind exposition index.

5 Discussion

It is known[2] that topography controls the thermal, wind, and hydrological regimes of slopes, influencing therefore the distribution and properties of soils and vegetation (Huggett and Cheesman, 2002; Florinsky, 2025a).

The thermal regime of slopes depends in part on the incidence of solar rays to the land surface, so it depends on both *G* and *A*. *TIns* directly considers this incidence and better describes the thermal regime (Böhner and Antonić, 2009). Information on the differentiation of slopes by insolation level is critical to predict the spatial distribution of primitive soils and lower plants in ice-free areas. To refine such a prediction, one can use *TWI* digital models describing topographic prerequisites of water migration and accumulation.

A further refinement of such a prediction can be done with *WEx* data. *WEx* digital models are utilized to identify areas affected by and protected from the wind impact (Böhner and Antonić, 2009; Florinsky, 2025a, chap. 2). In periglacial Antarctic landscapes, one of the main meteorological factors determining the microclimate is katabatic wind. Thus, *WEx* maps may be of great importance for modeling the distribution of primitive soil and lower plants, predicting the differentiation of snow accumulation in ice-free areas, and determining the optimal location of buildings and infrastructure at polar stations.

k_h maps display the distribution of convergence and divergence areas of surface flows. Geomorphologically, these are spurs of valleys and crests, respectively. The combination of convergence and divergence areas creates an image of the flow structures (Florinsky, 2025a, chap. 2). k_v maps show the distribution of relative deceleration and acceleration areas of surface flows. Geomorphologically, these maps represent cliffs, scarps, terrace edges, and other similar landforms or their elements with sharp bends in the slope profile (Florinsky, 2025a, chap. 2). In this regard, k_h and k_v digital models may be useful in geomorphological and hydrological studies of the ice-free areas.

Combination of k_h and k_v digital models allows revealing relative accumulation zones of surface flows (Florinsky, 2025a, chap. 2). These zones, marked by both $k_h < 0$ and $k_v < 0$, coincide with the fault intersection sites and are characterized by increased rock fragmentation and permeability. Within these zones, one can observe an interaction and exchange between two types of substance flows: (a) lateral, gravity-driven substance flows moved along the land surface and in the near-surface layer, such as water, dissolved and suspended substances, and (b) vertical, upward substance flows, such as fluids, groundwater of different mineralization and temperature (Florinsky, 2025a, chap. 15). Maps of accumulation zones may be useful for geochemical studies in the ice-free areas.

k_{max} and k_{min} maps are informative in terms of structural geology because they clearly display elongated linear landforms (Florinsky, 2017, 2025a). In Antarctica, such lineaments can be interpreted as a reflection of the local fault and fracture network, which topographic manifestation has been amplified by erosional, exaration, and nival processes (Florinsky, 2023b; Florinsky and Zharnova, 2025a). Thus, researchers are able to use k_{max} and k_{min} models for compiling lineament maps and comparing them with other geological data.

CA maps can be used to identify the fine flow structure of drainage basins and then to incorporate this information into geochemical and hydrological analysis. *TWI* digital models can be applied for prediction of the ground moisture content in the ice-free areas as well as for forecasting the spatial distribution of snow puddles on adjacent glaciers in summer. *SPI* data can be useful for prediction of slope erosion in the ice-free areas as well as erosion of snow cover and ice by meltwater flows on adjacent glaciers in summer.

[2] This one-page explanation of the usefulness and possible application of morphometric models and maps in Antarctic research has earlier been published in our papers on ice-free geomorphometry of Antarctica (Florinsky, 2025b; Florinsky and Zharnova, 2025b).

6 Conclusions

We performed geomorphometric modeling of the key ice-free areas of the Prince Olav Coast (Queen Maud Land, East Antarctica). For the first time, we created three series of morphometric models and maps for the Cape Hinode, Polkanov Hills (Cape Ryûgû), and Tereshkova Oasis (Sinnan Rocks).

The obtained maps rigorously, quantitatively, and reproducibly describe the ice-free topography of the Prince Olav Coast. New morphometric data can be used in further geological, geomorphological, glaciological, hydrological, and ecological studies of this Antarctic region.

The study was performed within the framework of the project for creating a physical geographical thematic scientific reference geomorphometric atlas of ice-free areas of Antarctica (Florinsky, 2024, 2025b).

References

Alexandrov MV (1973) Physical geographical features and morphology of the landscape of the Polkanov Oasis. Proceedings of the Soviet Antarctic Expedition 61:191–219 (in Russian).

Alexandrov MV (1985) Landscape structure and mapping of the Enderby Land oases. Hydrometeoizdat, Leningrad, USSR, 152 p. (in Russian).

Bakaev VG, Tolstikov EI (eds) (1966) Atlas of Antarctica, vol. I. Central Board of Geodesy and Cartography, Moscow–Leningrad, USSR, 241 p. (in Russian).

Beyer L, Bölter M (eds) (2002) Geoecology of Antarctic ice-free coastal landscapes. Springer, Berlin, Germany, 429 p. https://doi.org/10.1007/978-3-642-56318-8.

Böhner J (2004) Regionalisierung bodenrelevanter Klimaparameter für das Niedersächsische Landesamt für Bodenforschung (NLfB) und die Bundesanstalt für Geowissenschaften und Rohstoffe (BGR). Arbeitshefte Boden 4:17–66.

Böhner J, Antonić O (2009) Land-surface parameters specific to topo-climatology. In: Hengl T, Reuter HI (eds) Geomorphometry: concepts, software, applications. Elsevier, Amsterdam, the Netherlands, pp. 195–226. https://doi.org/10.1016/S0166-2481(08)00008-1.

Conrad O, Bechtel B, Bock M, Dietrich H, Fischer E, Gerlitz L et al. (2015) System for Automated Geoscientific Analyses (SAGA) v. 2.1.4. Geoscientific Model Development 8:1991–2007. https://doi.org/10.5194/gmd-8-1991-2015.

Donidze GI (ed) (1987) Dictionary of Antarctic geographic names. Central Scientific Research Institute for Geodesy, Aerophotosurveying, and Cartography, Moscow, USSR, 407 p. (in Russian).

ESA (2025) Sentinel-2. European Space Agency. https://sentiwiki.copernicus.eu/web/sentinel-2 (accessed 14 Aug. 2025).

ESRI (2015–2024) ArcGIS Pro. Environmental Systems Research Institute. https://www.esri.com/en-us/arcgis/products/arcgis-pro/overview (accessed 14 Aug. 2025).

Evans IS (1972) General geomorphometry, derivations of altitude, and descriptive statistics. In: Chorley RJ (ed) Spatial analysis in geomorphology. Methuen, London, UK, pp. 17–90.

Evans IS (1980) An integrated system of terrain analysis and slope mapping. Zeitschrift für Geomorphologie Suppl. 36:274–295.

Florinsky IV (2017) An illustrated introduction to general geomorphometry. Progress in Physical Geography 41:723–752. https://doi.org/10.1177/0309133317733667.

Florinsky IV (2023a) Geomorphometric modeling and mapping of Antarctic oases. arXiv:2305.07523 [physics.geo-ph], 84 p. https://doi.org/10.48550/arXiv.2305.07523.

Florinsky IV (2023b) Larsemann Hills: geomorphometric modeling and mapping. Polar Science 38:100969. https://doi.org/10.1016/j.polar.2023.100969.

Florinsky IV (2024) A project of a geomorphometric atlas of ice-free Antarctic territories. InterCarto. InterGIS 30(2):53–79 (in Russian, with English abstract) https://doi.org/10.35595/2414-9179-2024-2-30-53-79.

Florinsky IV (2025a) Digital terrain analysis, 3rd rev. enl. edn. Academic Press, London, UK ,455 p. https://doi.org/10.1016/C2023-0-51092-4.

Florinsky IV (2025b) Geomorphometric atlas of ice-free Antarctic areas: problem statement, concept,

and key principles. arXiv:2508.02846 [physics.geo-ph], 33 p. https://doi.org/10.48550/arXiv.2508.02846.
Florinsky IV, Zharnova SO (2025a) Geomorphometry of the Bunger Hills, East Antarctica. Advances in Polar Science 36:95–112. https://doi.org/10.12429/j.advps.2024.0042.
Florinsky IV, Zharnova SO (2025b) Ice-free geomorphometry of Queen Maud Land, East Antarctica: 1. Sôya Coast. arXiv:2508.10462 [physics.geo-ph], 89 p. https://doi.org/10.48550/arXiv.2508.10462.
GSI (1990) Prince Olav Coast. 1:250,000 Series. Geographical Survey Institute, Japan, 1 chart.
Hengl T, Reuter HI (eds) (2009) Geomorphometry: concepts, software, applications. Elsevier, Amsterdam, the Netherlands, 796 p.
Hiroi Y, Shiraishi K, Yoshida Y (1983) Explanatory text of geological map of Sinnan Rocks, Antarctica. Antarctic Geological Map Series, Sheet 14: Sinnan Rocks. National Institute of Polar Research, Tokyo, Japan, 7 p., 1 chart.
Howat IM, Porter C, Smith BE, Noh M-J, Morin P (2019) The Reference Elevation Model of Antarctica. Cryosphere 13:665–674. https://doi.org/10.5194/tc-13-665-2019.
Howat I, Porter C, Noh M-J, Husby E, Khuvis S, Danish E et al. (2022) The Reference Elevation Model of Antarctica – mosaics, version 2. Harvard Dataverse, V1, https://doi.org/10.7910/DVN/EBW8UC.
Huggett RJ, Cheesman J (2002) Topography and the environment. Pearson Education, Harlow, UK, 274 p.
Kamenev EN, Klimov LV, Shulyatin OG (1965) Geological structure of Enderby Land and Prince Olav Coast. In: Bugaev VA (ed), Antarctica. Reports of the Commission 1964. Nauka, Moscow, USSR, pp. 5–27 (in Russian).
Klimov LV (1965) Geological research in the area of the Prince Olav Coast in 1964. Information Bulletin of the Soviet Antarctic Expedition 51:55–63 (in Russian).
Korotkevich ES (1972) Polar deserts. Hydrometeoizdat, Leningrad, USSR, 419 p. (in Russian).
Korotkevich ES, Fomchenko VD, Friedman BS (eds) (2005) Atlas of the oceans: Antarctica. Head Department of Navigation and Oceanography, Arctic and Antarctic Research Institute, St. Petersburg, Russia, 280 p. (in Russian, with English contents, summary, and index).
Kovaleva OV (2014) Perfecting the representation of topography by hypsometric tints. New classification of hypsometric scales. Geodesy and Cartography 75(11):21–29 (in Russian, with English abstract). https://doi.org/10.22389/0016-7126-2014-893-11-21-29.
Markov KK, Bardin VI, Orlov AI (1962) Physio-geographical description of the coast line of East Antarctica. Moscow University Press, Moscow, USSR (in Russian, with English contents, preface, and conclusions).
Markov KK, Bardin VI, Lebedev VL, Orlov AI, Suetova IA (1970) The geography of Antarctica. Israel Program for Scientific Translations, Jerusalem, Israel, 370 p.
Minár J, Krcho J, Evans IS (2016) Geomorphometry: quantitative land-surface analysis. In: Elias SA (ed) Reference module in earth systems and environmental sciences. Elsevier, Amsterdam, the Netherlands. https://doi.org/10.1016/B978-0-12-409548-9.10260-X.
Moore ID, Grayson RB, Ladson AR (1991) Digital terrain modelling: a review of hydrological, geomorphological and biological applications. Hydrological Processes 5:3–30. https://doi.org/10.1002/hyp.3360050103.
Nakai Y, Kano T, Yoshikura S (1979) Outline of geology of Cape Ryûgû, Oku-iwa Rock and Telen, East Antarctica. Memoirs of National Institute of Polar Research 14:121–127.
Nakai Y, Kano T, Yoshikura S (1980) Explanatory text of geological map of Cape Ryûgû, Antarctica. Antarctic Geological Map Series, Sheet 15: Cape Ryûgû. National Institute of Polar Research, Tokyo, Japan, 9 p., 1 chart.
Patterson T, Jenny B (2011) The development and rationale of cross-blended hypsometric tints. Cartographic Perspectives 69:31–45. https://doi.org/10.14714/CP69.20.
Pickard J (ed) (1986) Antarctic oasis: terrestrial environment and history of the Vestfold Hills. Academic Press, New York, NY, 367 p.
PGC (2022–2024) REMA Exployer. Polar Geospatial Center, University of Minnesota, Saint Paul, MN. https://rema.apps.pgc.umn.edu (accessed 14 Aug. 2025).
Segal DB (1982) Theoretical basis for differentiation of ferric-iron bearing minerals, using Landsat MSS data. In: Proceedings of Symposium for Remote Sensing of Environment, 2nd Thematic

Conference on Remote Sensing for Exploratory Geology, Fort Worth, TX, pp. 949–951.
Shary PA, Sharaya LS, Mitusov AV (2002) Fundamental quantitative methods of land surface analysis. Geoderma 107:1–32. https://doi.org/10.1016/S0016-7061(01)00136-7.
Simonov IA (1971) Oases of East Antarctica. Hydrometeoizdat, Leningrad, USSR, 176 p. (in Russian).
Sokratova IN (2010) Antarctic oases: history and results of investigations. Arctic and Antarctic Research Institute, St. Petersburg, Russia, 274 p. (in Russian).
Tatsumi T, Kikuchi T (1959) Report of geomorphological and geological studies of the wintering team (1957–58) of the first Japanese Antarctic Research Expedition. Antarctic Record 7:373–388, 8:443–463 (in Japanese, with English abstract).
Tolstikov EI (ed) (1969) Atlas of Antarctica, vol. II. Hydrometeoizdat, Leningrad, USSR, 598 p. (in Russian).
Wilson JP and Gallant JC (eds) (2000) Terrain analysis: principles and applications. Wiley, New York, NY, 479 p.
Xu H (2006) Modification of normalised difference water index (NDWI) to enhance open water features in remotely sensed imagery. International Journal of Remote Sensing 27:3025–3033. https://doi.org/10.1080/01431160600589179.
Yanai K, Ishikawa T (1978) Explanatory text of geological map of Cape Hinode, Antarctica. Antarctic Geological Map Series, Sheet 11: Cape Hinode. National Institute of Polar Research, Tokyo, Japan, 6 p., 1 chart.
Yoshida Y (1983) Physiography of the Prince Olav and the Prince Harald Coasts, East Antarctica. Memoirs of National Institute of Polar Research, Ser. C: Earth Sciences 13:1–83.
Znachko-Yavorsky GA (1964) Brief lithological characteristics of the Quaternary deposits of the western part of Enderby Land. Information Bulletin of the Soviet Antarctic Expedition 49:5–8 (in Russian).
Znachko-Yavorsky GA, Klimov LV (1963) Main features of the topography of the western part of the Enderby Land. Information Bulletin of the Soviet Antarctic Expedition 41:11–13 (in Russian).

Appendix A

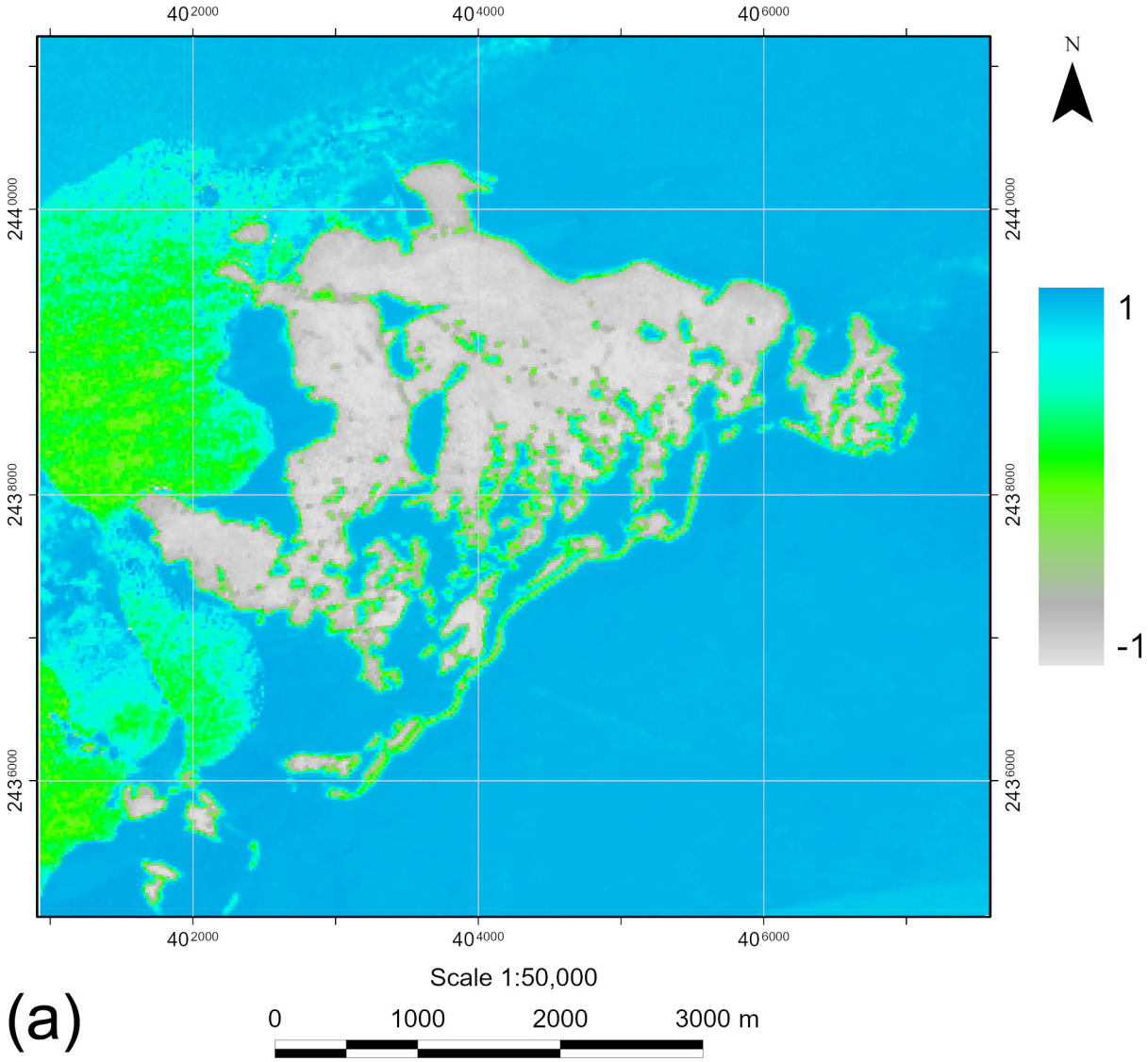

Fig. A1 MNDWI maps derived from Sentinel-2A MSI data: (a) Cape Hinode.

(Continued)

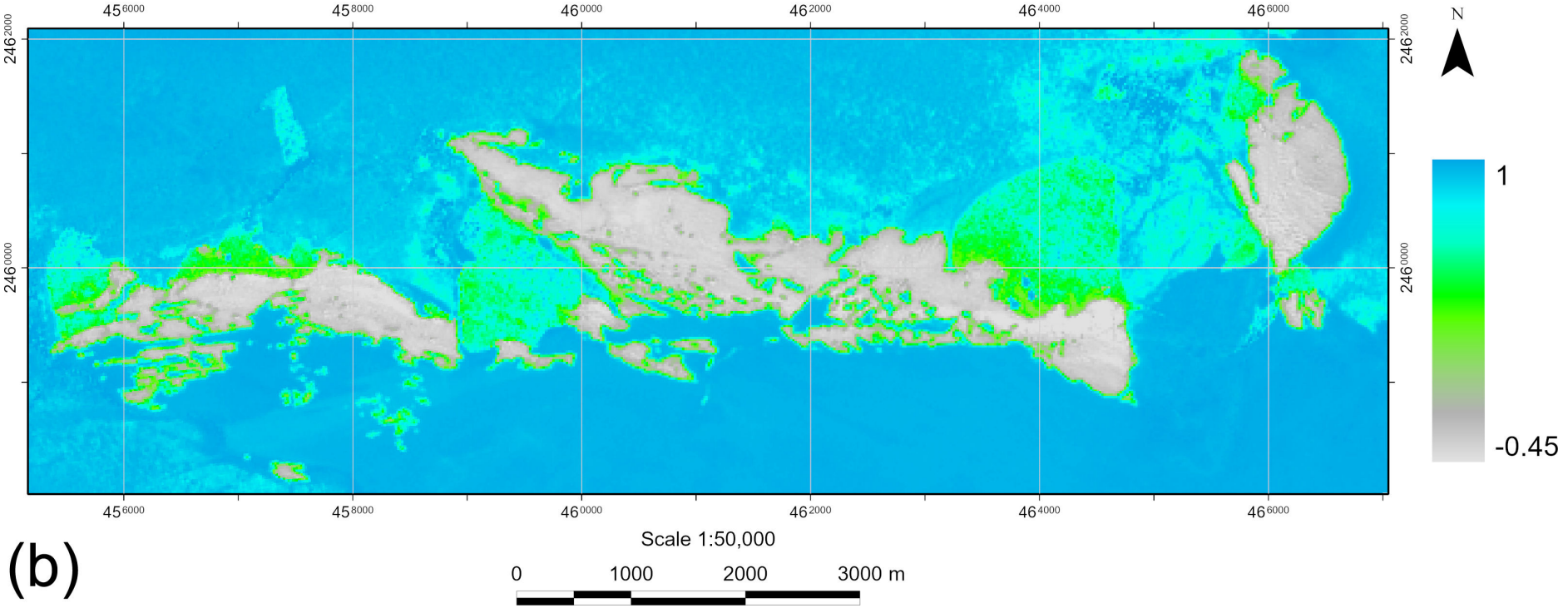

Fig. A1, cont'd MNDWI maps derived from Sentinel-2A MSI data: (b) Polkanov Hills (Cape Ryûgû).

(Continued)

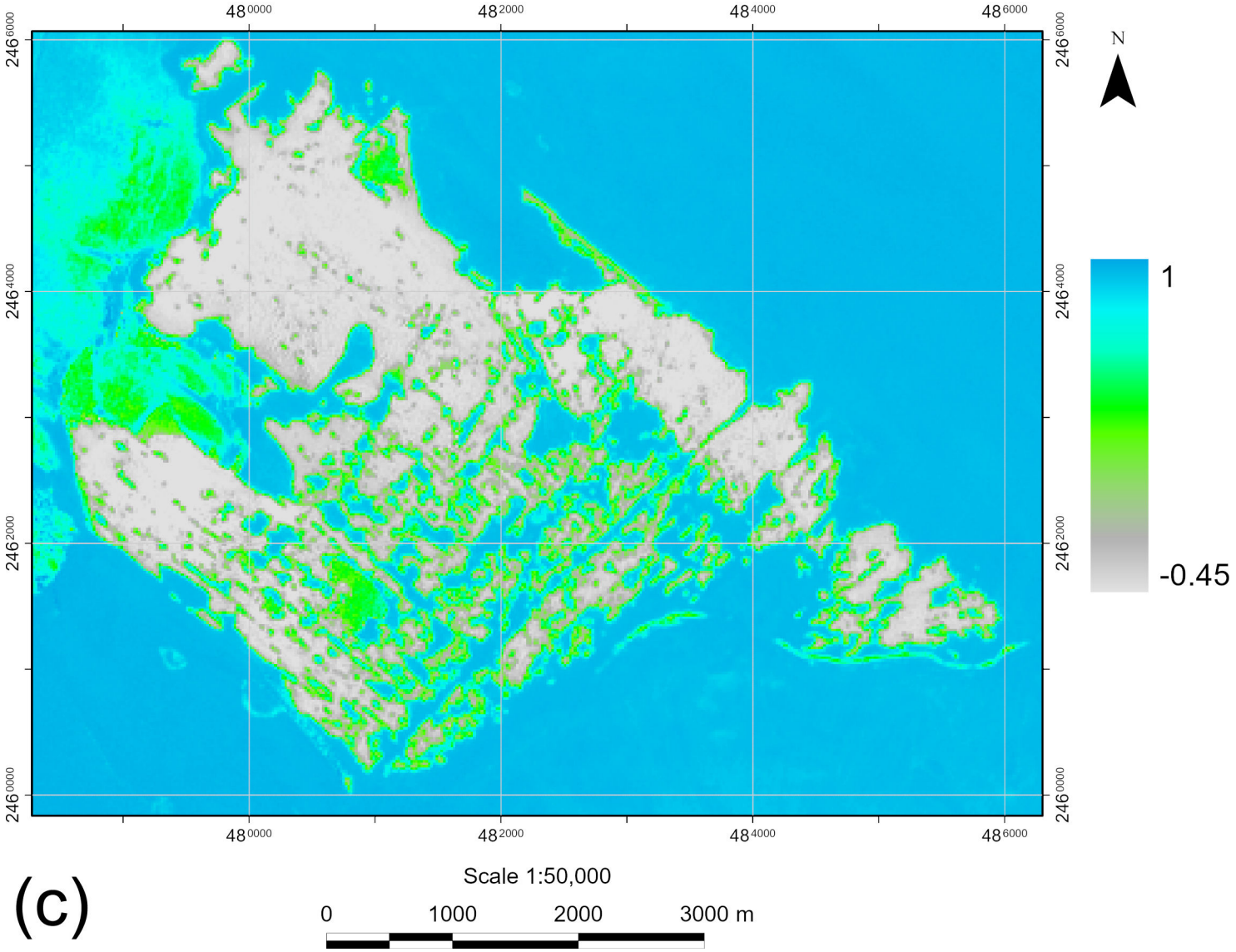

Fig. A1, cont'd MNDWI maps derived from Sentinel-2A MSI data: (c) Tereshkova Oasis (Sinnan Rocks).

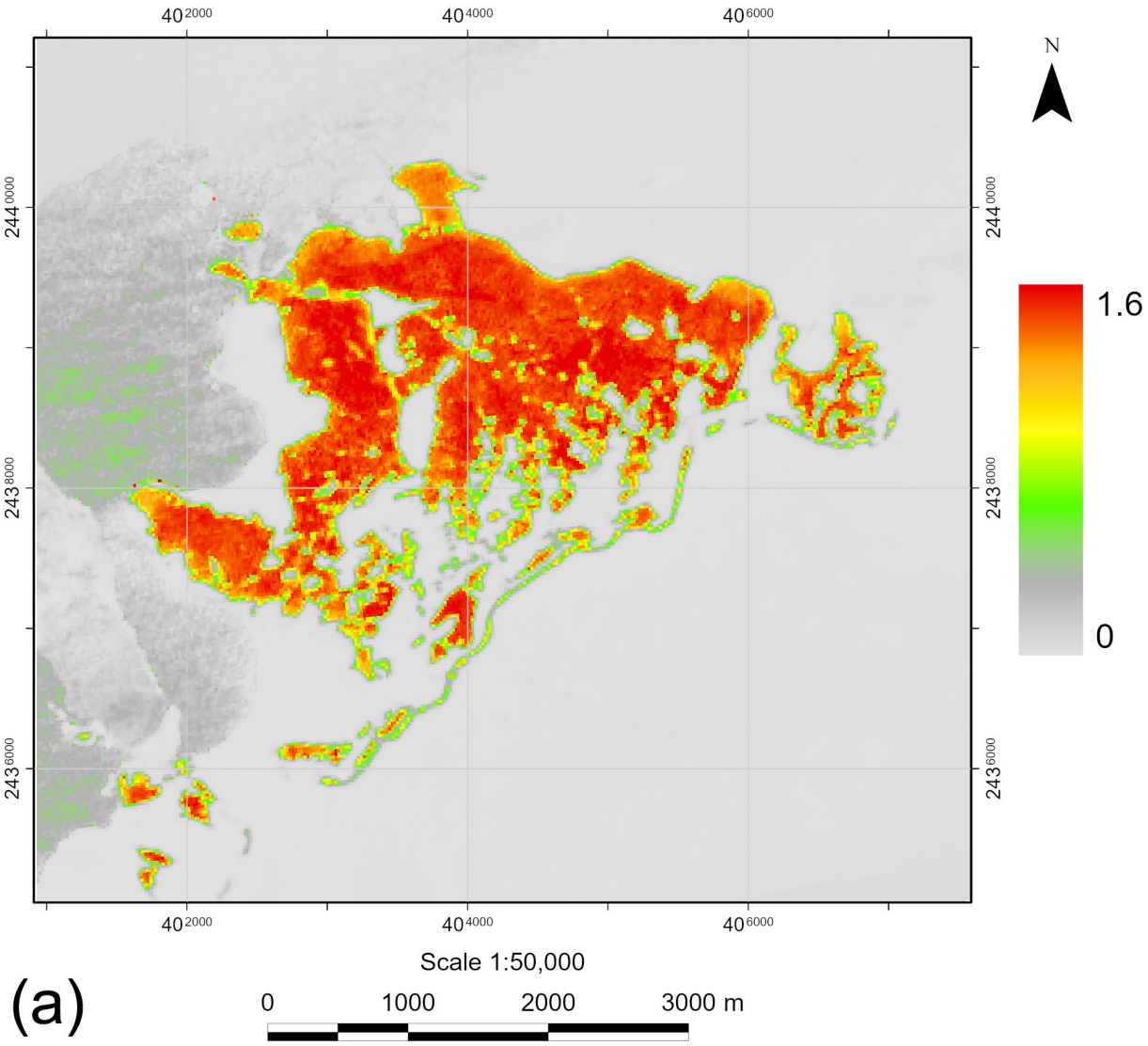

Fig. A2 FMR maps derived from Sentinel-2A MSI data: (a) Cape Hinode.

(Continued)

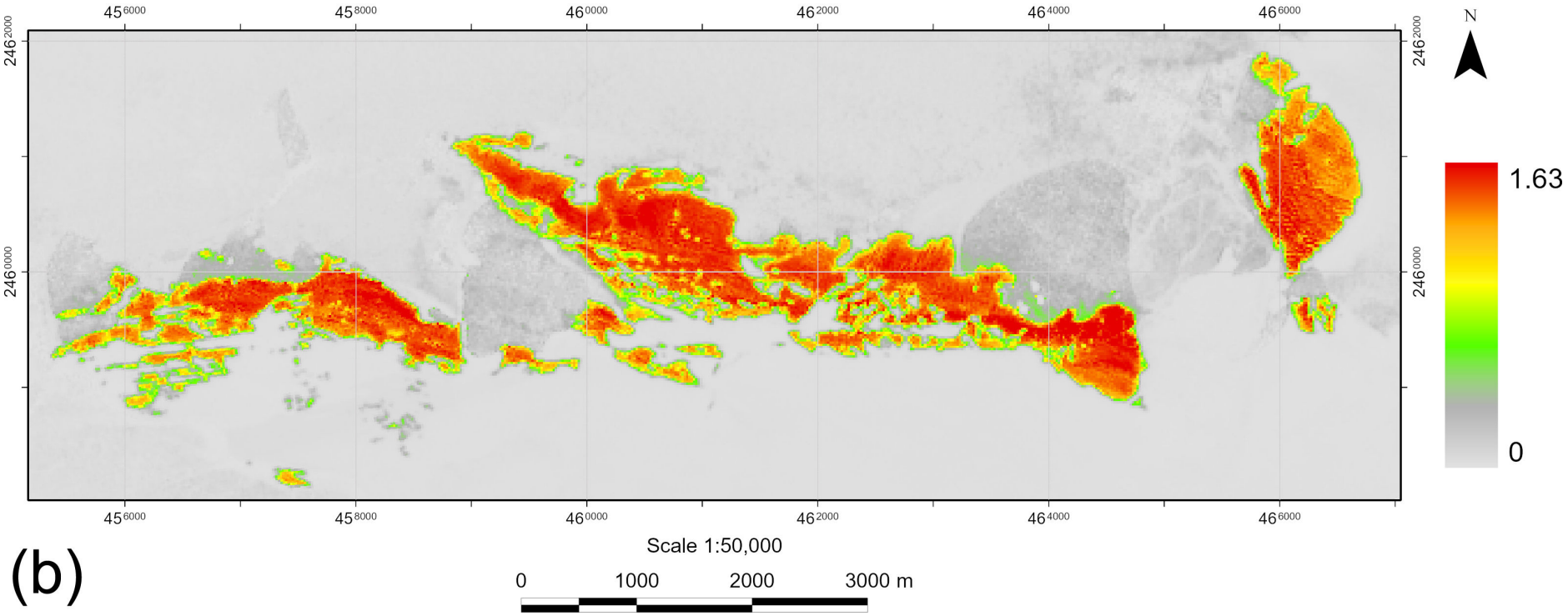

Fig. A2, cont'd FMR maps derived from Sentinel-2A MSI data: (b) Polkanov Hills (Cape Ryûgû).

(Continued)

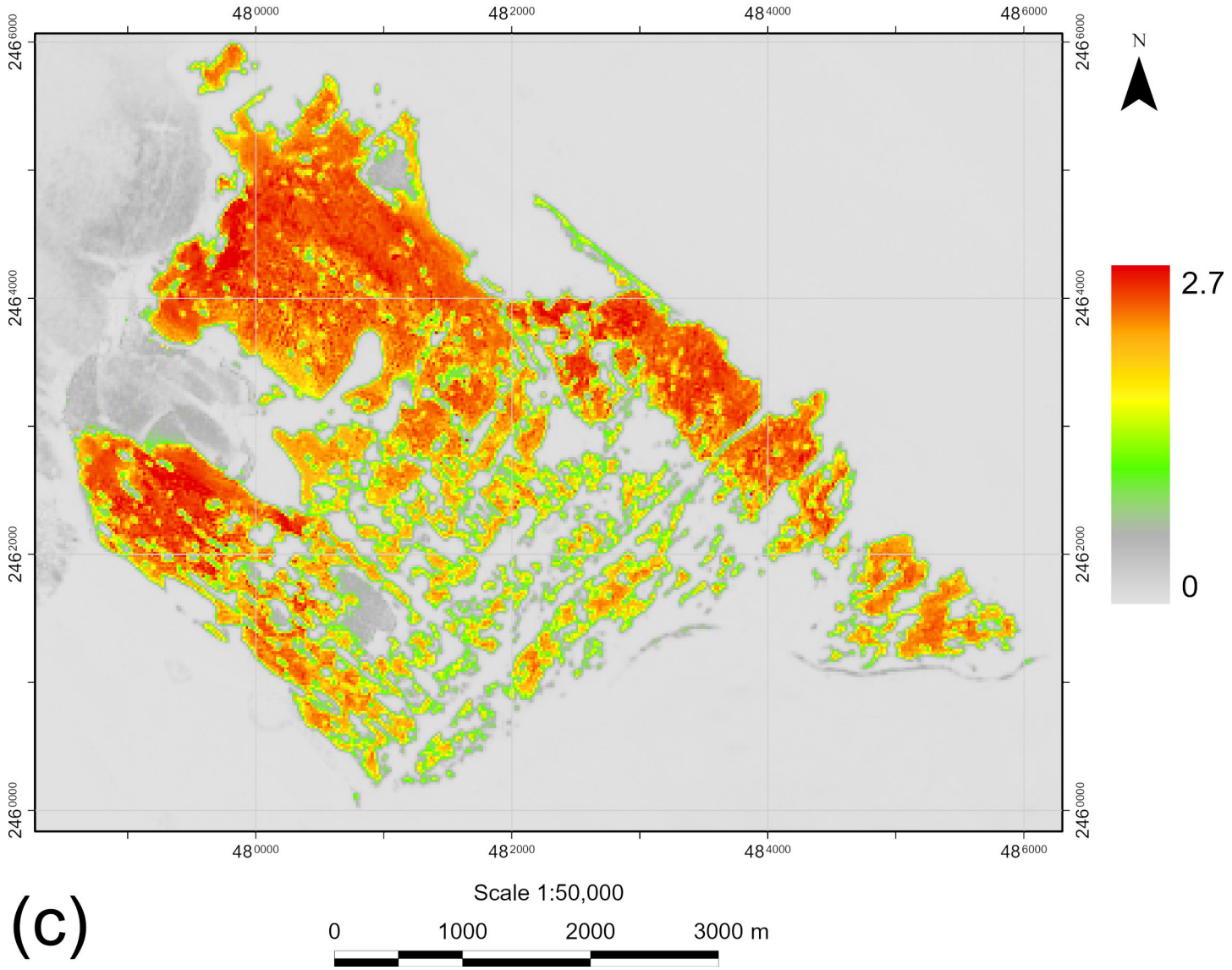

Fig. A2, cont'd FMR maps derived from Sentinel-2A MSI data: (c) Tereshkova Oasis (Sinnan Rocks).

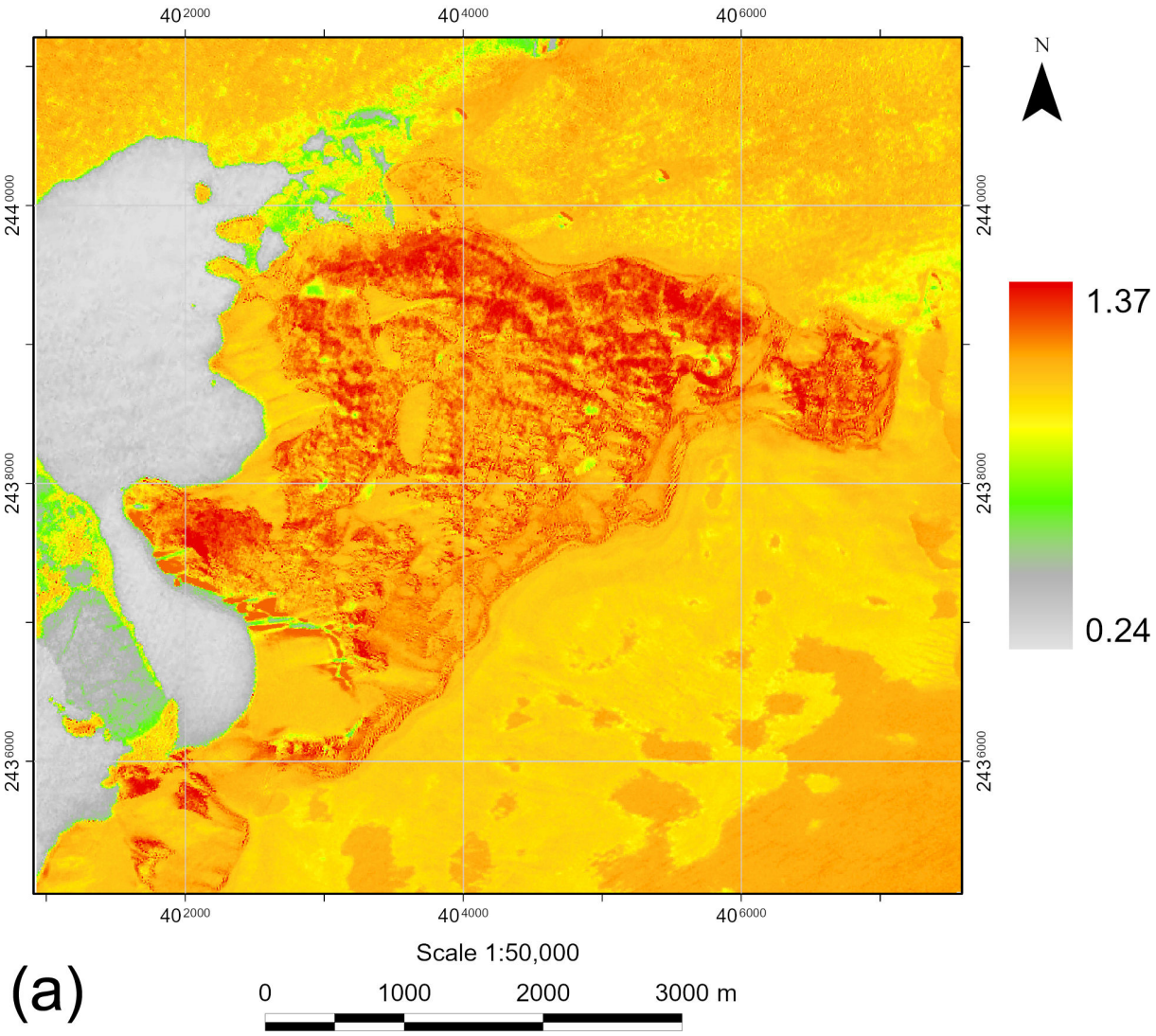

Fig. A3 IOR maps derived from Sentinel-2A MSI data: (a) Cape Hinode.

(Continued)

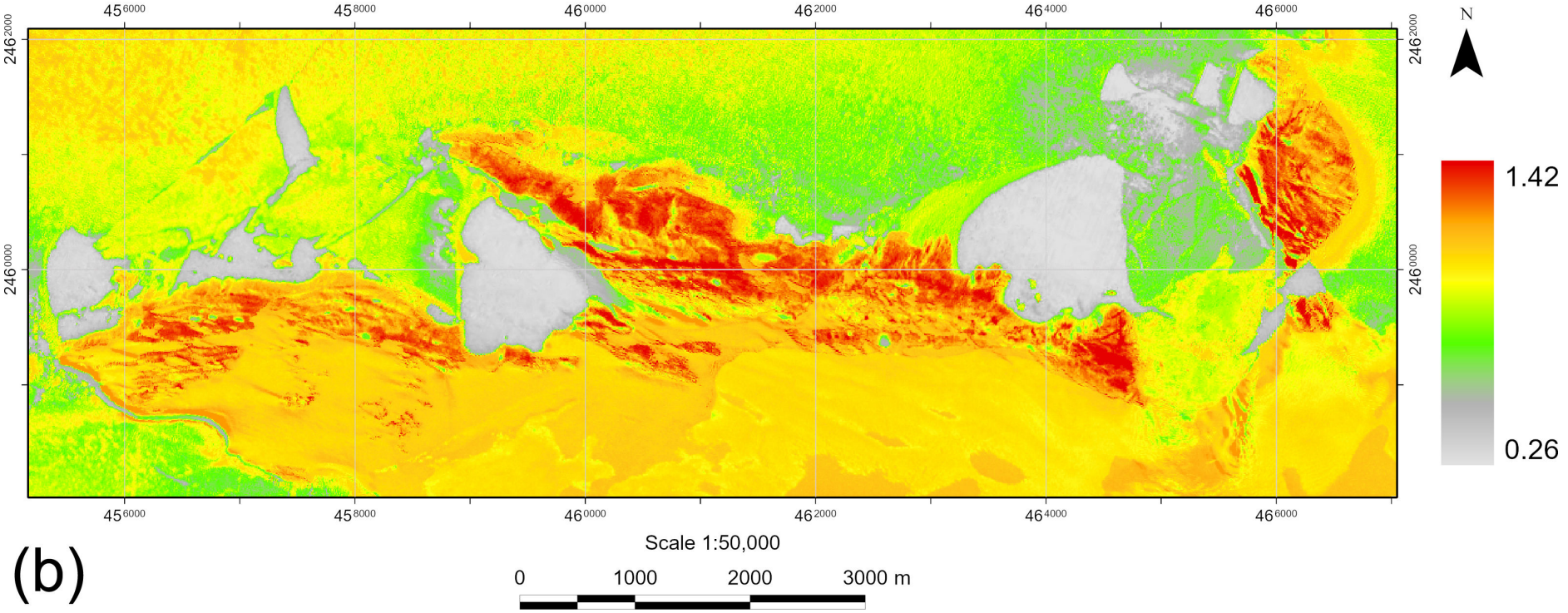

Fig. A3, cont'd IOR maps derived from Sentinel-2A MSI data: (b) Polkanov Hills (Cape Ryûgû).

(Continued)

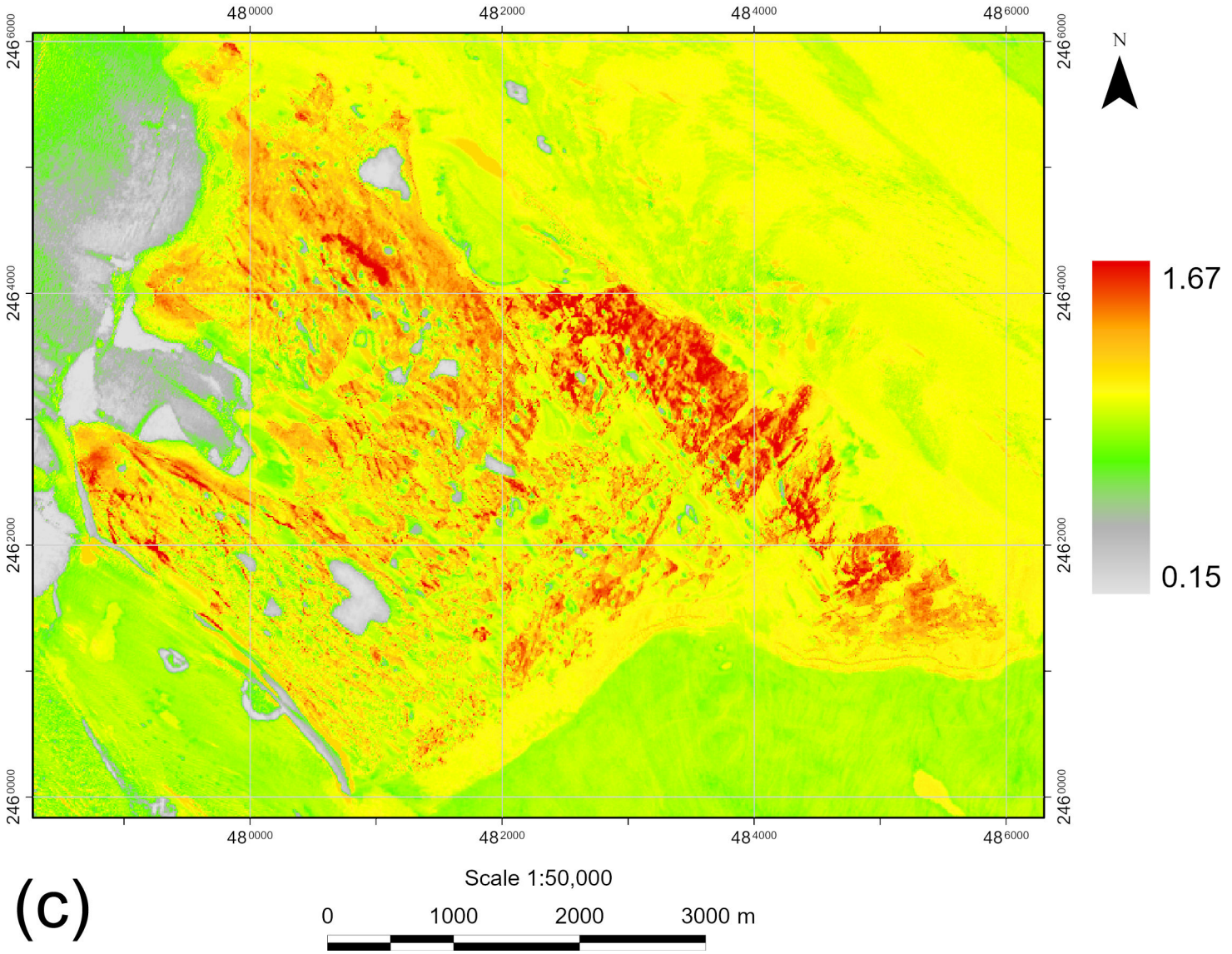

Fig. A3, cont'd IOR maps derived from Sentinel-2A MSI data: (c) Tereshkova Oasis (Sinnan Rocks).